國立交通大學

電子物理學系

碩 士 論 文

層狀二類超導體在強磁場的溫度–雜質相圖

Temperature-disorder phase diagram of layered type II superconductors in strong magnetic field by Monte Carlo simulation

研 究 生：謝博文

指導教授：儒森斯坦　教授

中 華 民 國 一百 年 六 月

層狀二類超導體在強磁場的溫度-雜質相圖

Temperature-disorder phase diagram of layered type II superconductors in strong magnetic field by Monte Carlo simulation

研 究 生：謝博文　　Student：Bo-Wen Xie

指導教授：儒森斯坦　教授　Advisor：Prof. Baruch Rosenstein

國立交通大學
電子物理學系
碩士論文

A Thesis
Submitted to Department of Computer and Information Science
College of Electrical Engineering and Computer Science
National Chiao Tung University
in partial Fulfillment of the Requirements
for the Degree of
Master
in

Electrophysics

Nov. 2010

Hsinchu, Taiwan, Republic of China

中華民國一百年六月

層狀二類超導體在強磁場的溫度-雜質像圖

學生：謝博文　　指導教授：如森斯坦　教授

國立交通大學電子物理研究所碩士班

摘要

在本論文中，我們使用二維金斯堡－朗道模型及準動量基底來模擬二維第二類超導體，並由蒙地卡羅方法來分析漩渦結構在熱擾和無序下的行為。我分析了在簡化溫度$a_T = -17 \sim -11$和無序常數$\zeta = 0 \sim 1$下的相變行為。藉由觀察平均後的傅立葉轉換的漩渦分布去分辨系統的相。並藉由比較 Y. Kato and N. Nagaosa 的蒙地卡羅模擬，在純淨系統下有限大小樣品的熔點，找出切確漩渦固態和漩渦液態的分界線。再由比較同樣兩種不同雜質分布的樣品，因為在雜質夠大情況下漩渦會固定在雜質上，所以可以藉此切確找出玻璃態的轉換線。

Temperature-disorder phase diagram of layered type II superconductors in strong magnetic field by Monte Carlo simulation

Student：Bo-Wen Xie **Advisor：Prof. Baruch Rosenstein**

Department of Electrophysics
National Chiao Tung University

ABSTRACT

The thermal fluctuations and disorder of vortices structure in highly anisotropic layered type II superconductors has been studied by Monte Carlo simulation in two dimensional Ginzburg-Landau model with the quasi-momentum basis. Vortices structure are studied with disorder parameter $\zeta = 0 \sim 1$ and reduced temperature $a_T = -17 \sim -11$ in the thesis. I developed the rotation averaging to analysis the snapshots of the Fourier transform of the superfluid density. I identified the melting line with disorder by comparing the vortices structure in pure system that the melting point of finite sample has been developed by Y. Kato and N. Nagaosa. And I identified the glass (irreversibility) line by comparing the difference of vortices structure with two different distribution of disorder. One can see the vortices pin on the disorder with disorder strong enough so that there are difference between the vortices structure with two different distribution of disorder to find the glass transition line. I will give a $a_T - \zeta$ phase diagram in the end.

Acknowledgement

首先要感謝我的指導教授，儒森斯坦老師，老師對學生總是細心指導，由淺入深、循序漸進的栽培我們。每當我遭遇瓶頸，老師也總是不吝嗇的指導我，教導我正面的研究態度，像我分享他的經驗和知識，在學短短兩年受益良多，老師諄諄教誨，使我銘感五內。接下來要感謝我的家人，家人總是默默的支持我，在物質上跟心靈上都給我很大的鼓勵，因為有家人的支持我才能順利的取得學位。最後要感謝在這兩年內給予我幫助的學長學姊與同學。

Contents

Figure List

Chapter 1

Introduction

1.1 Type II superconductor in magnetic field

Superconductors are materials that at sufficiently low temperatures possess such a remarkable properties as zero resistivity and perfect diamagnetism. One can divide superconductors into two different classes: Type I and Type II. Type I superconductors completely expel magnetic field (the Meissner effect) when they are under magnetic field lower than a certain critical magnetic field H_c and the superconductivity will be destroyed (including Meissner effect) at fields higher than H_c. Many metals belong to this class although typically critical temperature T_c at which the superconductivity appears is very low (below 10K). Higher critical temperatures are achieved in so called type II superconductors which are almost exclusively used in applications.

While early type II superconductors were also "low T_c" metals and alloys with temeratures about 10K, in 1986 new kind of such superconductors was discovered: cuprate high-temperature superconductors. The critical temperature exceeded 100K and attracted a wide spread interest to new phenomena in superconductivity such as thermal fluctuations and role of disorder. The important feature of the new superconductors is their layered structure, especially in Bi and Th based materials. The anisotropy is so high that the superconductivity is nearly two dimensional (2D). In this work I will study a 2D model of highly fluctuating superconductors subject to

magnetic field.

Magnetic properties of new superconductors are quite distinct. In a type II superconductors there are three regions in magnetic phase diagram, namely the T-H, divided by two critical magnetic field $\mathrm{H}_{c1}(T)$ and $\mathrm{H}_{c2}(T)$ as shown in Fig. 1-1-1. The Messner effect exists only when external magnetic field is below the lower critical field $\mathrm{H}_{c1}(T)$ and there the superconductors have no resistence. In the intermediate region, $\mathrm{H}_{c1}(T) < \mathrm{H} < \mathrm{H}_{c2}(T)$ certain amount of magnetic flux penetrates the superconductors in a form of fluxions carrying one unit of flux $\phi_0 = \frac{hc}{2e}$ also called Abrikosov vortices. In center of the vortex there is the normal core. The superconductivity is destroyed in the core of a smaller width ξ called the coherence length. Two major characteristics of the mixed state are the coherence length ξ which is the size of the normal core and the penetration depth λ on whose scale the supercurrent decays. The type II superconductivity refers to materials in which the ratio $\kappa = \frac{\lambda}{\xi}$ is larger than $\kappa_c = \frac{1}{\sqrt{2}}$ ([1] A. A. Abrikosov). For the strongly type II superconductors $\kappa \sim 100 \gg \kappa_c$, they are strongly fluctuating due to high T_c and large anisotropy in a sense that thermal fluctuations of the vortex degrees of freedom are not negligible.

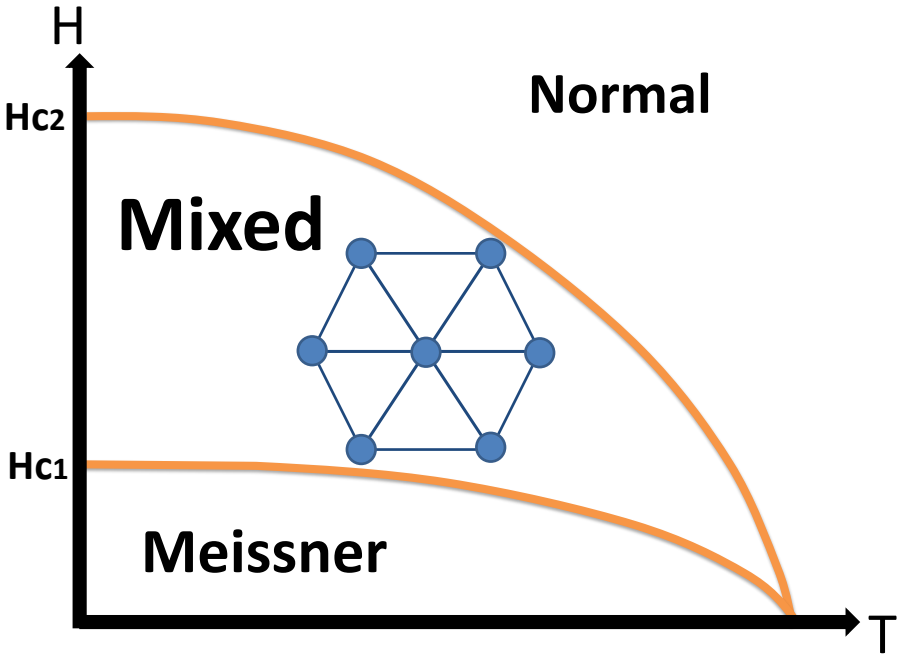

Fig. 1-1-1: Schematic magnetic phase diagram of type II superconductor.

1.2 Ginzburg - Landau model

Central to this theory is the introduction of the concept of an order parameter. The order parameter is an appropriate quantity which vanishes in the high temperature phase ($T > T_c$) but acquires a nonzero value below the transition ($T < T_c$). Treat superconductivity as a "spontaneously broken system" and some kind of macroscopic quantum state. Ginzburg and Landau built the idea that assume the existence of a macroscopic "wave function", ψ, which they took as the order parameter associated with superconductivity. It's much easier to explain type II superconductivity by this model that starting from phenomenology instead BCS theory starting from microscopic system.

The GL free energy near T_c undergoing a phase transition:

$$F[\psi] = \int d^3 \left\{ \frac{\hbar}{2m} \left| \left(\nabla - \frac{ie^*}{\hbar c} \vec{A} \right) \psi \right|^2 + a'(T)|\psi|^2 + b'(T)|\psi|^4 \right\}, \tag{1.2.1}$$

where $a'(T) = aT_c \left(1 - \frac{T}{T_c}\right)$ and $b'(T)$ are phenomenological parameters.

The coherence length and penetration depth are defined by

$$\xi^2(T) = \frac{\hbar^2}{2m\alpha(T_c - T)} \tag{1.2.2}$$

$$\lambda^2(T) = \frac{c^2 m\beta}{4\pi e^2 \alpha(T_c - T)} \tag{1.2.3}$$

1.3 Thermal fluctuations and disorder

Vortex Phases and The Properties

The phase diagram of superconductors in magnetic has been determined in details. By Ginzburg-Landau theory, the properties of superconductors is determined by the "distance" between the vortices. In the presence of thermal fluctuations in high Tc materials the vortex crystal melts into a vortex liquid as the external magnetic field $H \gg H_1$. A quantitative theory of thermal fluctuations using the lowest Landau level approximation is given. On the other hand, in the presence of quenched disorder pinning the vortex matter acquires certain "glassy" properties.

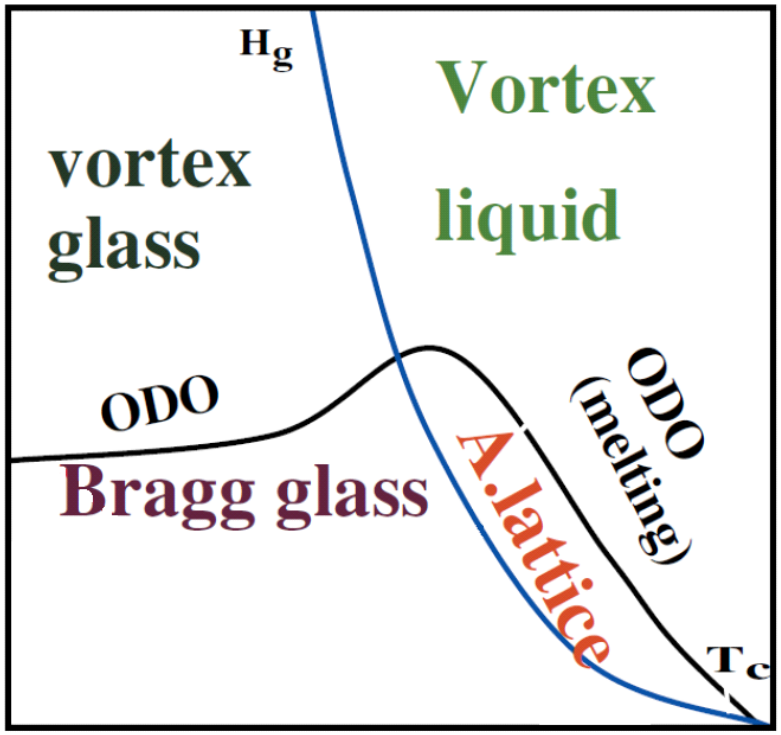

Fig. 1-3-1: Theoretical T-B phase diagram([2] B. Rosenstein).

Melting by thermal fluctuation

In high Tc superconductors temperature can be high enough, so that one cannot neglect additional thermal fluctuations which occur on the mesoscopic scale. The Ginzburg parameter,

$$G_i = 2\left(\frac{T_c}{16\pi F_{GL}\xi^2\xi_c}\right)^2 \qquad (1.3.1)$$

where $\xi_c = \gamma_a^{-1}\xi$ is the coherence length in the field direction, generally characterizes the strength of the thermal fluctuations on the mesoscopic scale([3] A. P Levanyuk; [4] V. L.Ginzburg; [5] Larkin). The definition of Gi is in the papers of D. P. Li and B. Rosenstein([6] D. Li and B. Rosenstein; [7] D. Li and B. Rosenstein). The Ginzburg parameter is significantly larger in high T_c superconductors compared to

the low temperature one. The physical reasons behind the enhancement are the small coherence length, high T_c and large anisotropy(γ_a in some case like BSCCO). Under these circumstances fluctuations influence various physical properties and even lead to new observable qualitative phenomena such as the vortex lattice melting into a vortex liquid. There are several remarkable experiments determined that the vortex lattice melting in high Tc superconductors is first order ([8] E. Zeldov; [9] M. Willemin; [10] T. Nishizaki; [11] H. Beidenkopf; [12] H. Beidenkopf) and spikes in specific heat ([13] A. Schilling; [14] A. Schilling; [10] T. Nishizaki; [15] F. Bouquet; [16] R. Lortz; [17] R. Lortz).

"Glassy" properties by disorder

In type II superconductivity, it will form vortices in superconductor if the external magnetic field is strong. There's dissipation because the magnetic field penetrate the superconductor and make the vortices moving. As the vortices pin on the impurities (pinning effect) the flux flow may be stopped and the material restores the property of zero resistivity. Otherwise thermal fluctuations might depin the vortices and make various quantities such as magnetization become irreversible. Disorder on the mesoscopic scale can be modeled in the framework of the Ginzburg- Landau approach adding a random component to its coefficients ([18] A. I. Larkin). The random component of the coefficient of the quadratic term $W(r)$ is called δT disorder since it can be interpreted as a local deviation of the critical temperature

from Tc.

$$a' \to a'[1 + W(r)], \qquad \overline{W(r)W(r')} = n\xi^2\xi_c\delta(r - r') \tag{1.3.2}$$

Disordered vortex matter is depinned at certain "critical current" Jc and the flux flow ensues. Close to Jc the flow proceeds slowly via propagation of elastic flow before becoming a fast plastic flow at larger currents. The I-V curves of the disordered vortex matter therefore are nonlinear. Disorder creates a variety of "glassy" properties involving slow relaxation, memory effects, etc.

1.4 Goals of the present work

Although most people believe the existence of the Abrikosov lattice phase that solved from GL equation by LLL approximation, but T. Giamarchi and P. Le Doussal disagree([19] T. Giamarchi). They claimed there's no Abrikosov phase by two approaching: gauge glass model([20] M. P. A. Fisher; [21] D. S. Fisher) and elastic lattice structure at small scale([22] M. Feigelman). Fig. 1-4-1 is the phase diagram of their prediction. I tried to plot the phase diagram by using Monte Carlo simulation. I analyzed the results of the MC simulation directly in mathematical way to check the phase diagram.

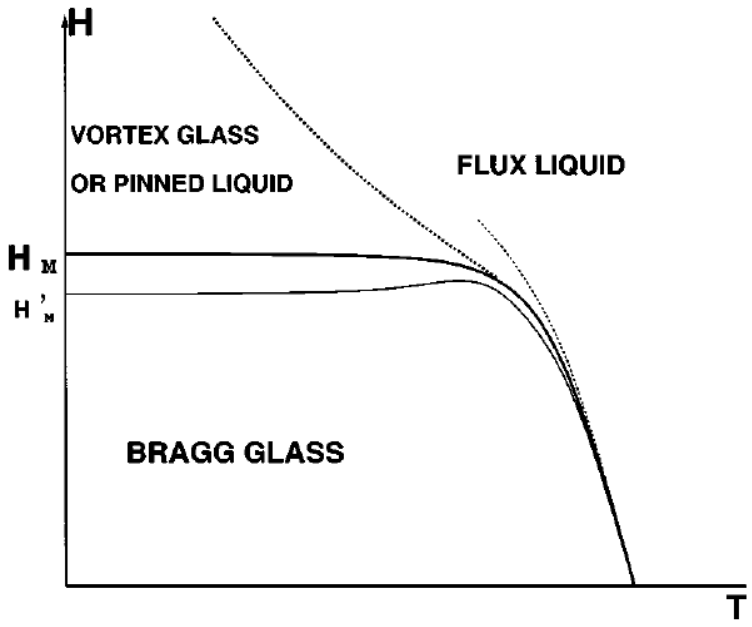

Fig. 1-4-1: The phase diagram by T. Giamarchi and P. Le Doussal's prediction([19] T. Giamarchi). Comparing with Fig. 1-3-1, one can find there's no Abrikosov phase in this phase diagram.

Chapter 2

Description of a layered superconductors in strong magnetic fields by the LLL approximation

2.1 Landau levels and the quasimomentum basis

We focuses on the properties of the two dimensional type II superconductors with the external magnetic field in the region $\mathrm{H}_{c1} \ll \mathrm{H} < \mathrm{H}_{c2}$ in the thesis. LLL approximation is the most acceptable theory where $\mathrm{H} \approx \mathrm{H}_{c2}$. In LLL theory, since magnetization is small we replace the field inside superconductor B by external field H which is essentially homogeneous. So we can drop the nonlinear term of the Ginzburg-Landau equation.

As the thermal fluctuations becoming strong enough, excitations of the lattice are no longer invariant under the symmetry transformations. So we need to regauge the system with LLL theory by the quasimomentum basis.

Solve the linear Ginzburg-Landau equation order parameter expanding in quasimomentum basis within the LLL([23] D. Li and B. Rosenstein)

$$\psi(\mathrm{x},\mathrm{y}) = \sum\nolimits_k C_k \varphi_k \tag{2.1.1}$$

$$\varphi_k = \sqrt{\frac{2\pi}{\sqrt{\pi}a}} \sum_{\kappa=-\infty}^{\infty} exp\left\{ i\left[\frac{\pi\kappa(\kappa-1)}{2} - \frac{2\pi\left(x-k_y\right)}{a}\kappa - xk_x \right] - \frac{1}{2}\left(y + k_x - \frac{2\pi}{a}\kappa \right)^2 \right\} \tag{2.1.2}$$

where the coefficients C_k are complex numbers and φ_k are quasi-momentum basis. We can find the property of φ_k

$$\varphi_k = \exp\{-ixk_x\}\varphi_0(x - k_y, y + k_x). \tag{2.1.3}$$

It is proved that quasi-momentum basis satisfy magnetic transitions([24] B. Rosenstein) which is defined as

$$\mathrm{T}_d\varphi_k = e^{i\boldsymbol{kd}}\varphi_k, \tag{2.1.4}$$

here $\mathbf{d}$ is the general displacement vector and T_d is magnetic translation operator. The sample size in the simulation is finite and had following dimensions([25] H. Y. Lin):

$$\mathbf{L} = \mathrm{L}\boldsymbol{d_1} + L\boldsymbol{d_2} \tag{2.1.5}$$

$$\boldsymbol{d_1} = (a, 0), \qquad \boldsymbol{d_2} = (\frac{1}{2}, \frac{\sqrt{3}}{2}) \tag{2.1.6}$$

here $\mathrm{a} = \sqrt{\frac{4\pi}{\sqrt{3}}}$. Thus, the area of the rectangle is $\mathrm{L}^2\boldsymbol{d_1} \times \boldsymbol{d_2} = 2\pi N_s,\ N_s = \mathrm{L}^2$.

According to definition of d_1 and d_2, the basis vector $\tilde{d}_1$ and $\tilde{d}_2$ of the reciprocal lattice are

$$\tilde{\boldsymbol{d}}_{\boldsymbol{1}} = \frac{2\pi}{a}\left(1, -\frac{1}{\sqrt{3}}\right), \qquad \tilde{\boldsymbol{d}}_{\boldsymbol{2}} = \frac{2\pi}{a}\left(0, \frac{2}{\sqrt{3}}\right) \tag{2.1.7}$$

We work in reciprocal lattice vector, so that $\boldsymbol{k}$ with the basis vector is

$$\boldsymbol{k} = \mathrm{k}_1\tilde{\boldsymbol{d}}_{\boldsymbol{1}} + \mathrm{k}_2\tilde{\boldsymbol{d}}_{\boldsymbol{2}} \tag{2.1.8}$$

Here $\mathrm{k}_1 = 0, \frac{1}{L}, \ldots, \frac{\mathrm{L}-1}{L}$ and $\mathrm{k}_2 = 0, \frac{1}{L}, \ldots, \frac{\mathrm{L}-1}{L}$ due to we choose the lowest Landau level wave function with quasi-momentum $\boldsymbol{k}$.

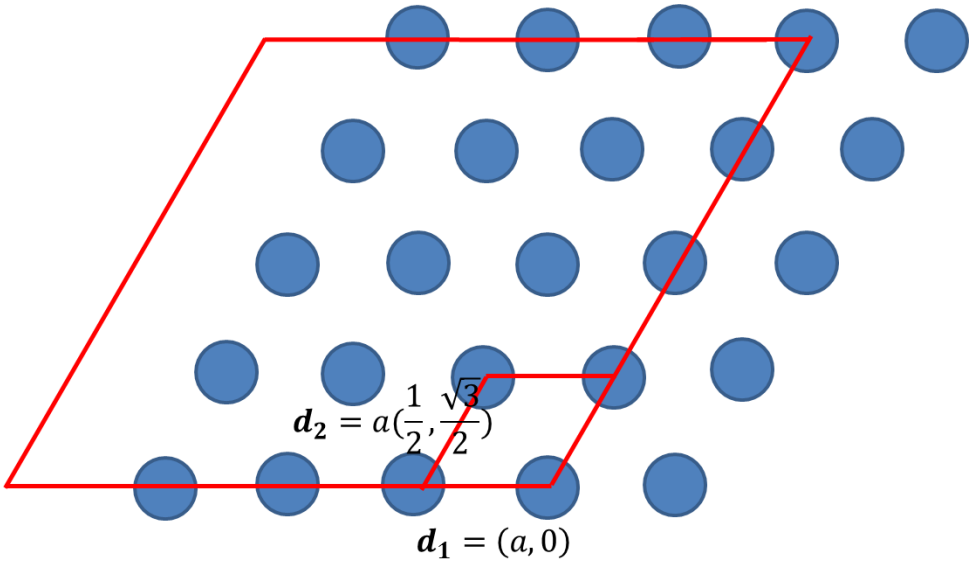

Fig. 2-1-1: Interpretation of the lattice vector d_1 and d_2.
a is the distance of a vortex to another adjacent vortex.

The quasi-momentum basis satisfy magnetic translations

$$\mathrm{T}_L\psi(x,y) = e^{ikL}\psi(x,y), \tag{2.1.9}$$

and then we have

$$e^{ikL} = 1$$

$$\mathrm{k}_x = \frac{2\pi}{L}n_x, \qquad n_x = 0, \pm 1, \pm 2, \ldots$$

$$\mathrm{k}_y = \frac{2\pi}{L}n_y, \qquad n_y = 0, \pm 1, \pm 2, \ldots \tag{2.1.10}$$

Because of using the LLL approximation, the ranges of n_x and n_y are

$$n_x = 0,1, \ldots, L-1$$

$$n_y = 0,1, \ldots, L-1 \tag{2.1.11}$$

2.2 Free energy

We start at the two dimensional GL free energy:

$$\mathrm{F} = \int dxdy \frac{\hbar}{2m}\left|\left(\nabla - \frac{\mathrm{ie}^*}{\hbar c}\boldsymbol{A}\right)\psi\right|^2 + \alpha'(T)\big(1 + U(x,y)\big)|\psi|^2 + \frac{b'(T)}{2}|\psi|^2 \quad (2.2.1)$$

where ψ is the order parameter of the superconductivity, $\boldsymbol{A}$ is the magmetic vector potential. m and e^* are the mass and charge of the Cooper pair. $\alpha'(T) = \alpha T_c(1-t)$ and $b'(T)$ are phenomenological parameters. $U(x,y)$, the disorder term, is like $\mathrm{W(r)}$ which is the disorder coefficient by Larkin ([18] A. I. Larkin).

$$\overline{U(x,y)U(0,0)} = R\delta(x)\delta(y) \quad (2.2.2)$$

Let us focus the clean system first. The GL free energy equation for pure vortex system is

$$\mathrm{F} = \int dxdy \frac{\hbar}{2m}\left|\left(\nabla - \frac{\mathrm{ie}^*}{\hbar c}\boldsymbol{A}\right)\psi\right|^2 + \alpha'(T)|\psi|^2 + \frac{b'(T)}{2}|\psi|^4 \quad (2.2.3)$$

In order to get the dimensionless LLL free energy, we need to rescale $\psi^2 \rightarrow \sqrt{\frac{T}{l^2 b' 4\pi}}\psi^2$, $\mathrm{x} \rightarrow \frac{\mathrm{x}}{l}$, $\mathrm{y} \rightarrow \frac{\mathrm{y}}{l}$ and $l = \frac{\xi}{\sqrt{B/H_{c_2}}}$, then we obtain in

$$\frac{\mathrm{F}}{T} = \frac{1}{4\pi}\int dxdy\left[a_T|\psi|^2 + \frac{1}{2}|\psi|^4\right] \quad (2.2.4)$$

here,

$$a_T = \frac{2\alpha_\beta \pi^{1/2} l}{b'^{1/2} T^{1/2}} \quad (2.2.5)$$

is the reduced temperature, and $\alpha_\beta = \alpha T_c(1-b-t)$.

Here is the GL free energy in the form that we'll use it in Monte Carlo simulation. The Gaussian integrals referred to the paper of B. Rosenstein and D. Li ([24] B.

Rosenstein) is

$$\int_{\boldsymbol{r}} dx\varphi(\boldsymbol{r})\varphi_{\boldsymbol{k}}^{*}(\boldsymbol{r})\exp[-i\boldsymbol{r}\cdot\boldsymbol{q}] = 4\pi\sum_{Q_1,Q_2}\delta(\boldsymbol{q}-\boldsymbol{k}-\boldsymbol{Q})\,F(\boldsymbol{k},\boldsymbol{Q}) \tag{2.2.6}$$

here

$$F(\boldsymbol{k},\boldsymbol{Q}) = exp\left\{-\frac{q^2}{4}+i\left[\left(\frac{\pi}{2}\right)Q_1^2-\left(\frac{q_xq_y}{2}\right)+k_xq_y\right]\right\} \tag{2.2.7}$$

with decomposition of arbitrary momentum q into its rational part $\boldsymbol{k}$, which belongs to the Brillion zone, and an integer part $\boldsymbol{Q}$, belonging to the reciprocal lattice

$$\boldsymbol{q} = \boldsymbol{k}+\boldsymbol{Q}, \qquad \boldsymbol{Q} = Q_1\tilde{\boldsymbol{d}}_{\boldsymbol{1}}+Q_2\tilde{\boldsymbol{d}}_{\boldsymbol{2}} \tag{2.2.8}$$

The inverse Fourier transform of Eq. (2.2.6) is

$$\varphi(\boldsymbol{r})\varphi_{\boldsymbol{k}}^{*}(\boldsymbol{r}) = \sum_{\boldsymbol{Q}}\exp[i(\boldsymbol{k}+\boldsymbol{Q})\cdot\boldsymbol{r}]\exp\left[\frac{\pi i}{2}(Q_1^2+Q_1)\right]exp\left[-\frac{(\boldsymbol{k}+\boldsymbol{Q})^2}{4}\right. \tag{2.2.9}$$
$$\left.-\frac{i(k_x+Q_x)(k_y+Q_y)}{2}+ik_x(k_y+Q_y)\right]$$

Since the superfluid density and its Fourier transform defined as:

$$\rho(\mathrm{x},\mathrm{y}) = |\psi(x,y)|^2 = \sum_{k,l}C_kC_l\varphi_k\varphi_l \tag{2.2.10}$$

$$\tilde{\rho}(\mathbf{p}+\mathbf{P}) = \frac{1}{2\pi L^2}\int exp[-i(\boldsymbol{p}+\boldsymbol{P})\cdot\boldsymbol{r}]\times\rho(x,y)\,dxdy \tag{2.2.11}$$

From the equations from Eq. (2.2.6) to Eq. (2.2.11) we get the quadratic term in Eq. (2.2.4)

$$\frac{1}{4\pi}\int_{x,y}a_T|\psi(x,y)|^2 = \frac{a_T}{2}L^2\sum_l C_l^*C_l \tag{2.2.12}$$

while the quartic term takes a form

$$\frac{1}{8\pi}\int_{x,y}|\psi(x,y)|^4 \tag{2.2.13}$$

$$= \frac{1}{4}L^2\sum_{\boldsymbol{p},\boldsymbol{P}}\left|\sum_{l} exp\left\{i\pi\left[-P'(2l_2-l_1)+\frac{1}{2}(p_1+2l_1\right.\right.\right.$$

$$\left.\left.\left.-P'')[2(p_2+P_2)-(p_1+P_1)]\right]\right\} exp\left[\frac{i\pi}{2}(P'^2\right.$$

$$\left.-P')\right] exp\left[-\frac{(\boldsymbol{p}+\boldsymbol{P})^2}{4}\right] C^*_{[p_1+l_1],[p_2+l_2]}C_l\Bigg|^2$$

The disordered term of the GL free energy is

$$\int_{x,y}\alpha T_c(1-t)U(x,y)|\psi|^2 \tag{2.2.14}$$

$$= 2\pi L^2\frac{l\alpha T_c(1-t)}{2(\pi b'T)^{\frac{1}{2}}}\left\{\tilde{\rho}(0)a_{0,0,0,0}\right.$$

$$+\sum_{p_1>0,P_1\geq 0,p_2=0,P_2=0}\left[\tilde{\rho}(\boldsymbol{p}+\boldsymbol{P})a^*_{p_1,0,P_1,0}+c.c.\right]$$

$$\left.+\sum_{p_2+P_2>0}\left[\tilde{\rho}(\boldsymbol{p}+\boldsymbol{P})a^*_{\boldsymbol{p},\boldsymbol{P}}+c.c.\right]\right\}$$

Where a is defined as random potential coefficient by Lin ([25] H. Y. Lin).

$$\mathrm{U}(x,y) = a_{0,0,0,0} \tag{2.2.15}$$

$$+\sum_{p_1>0,P_1\geq 0,p_2=0,P_2=0}\left\{a_{p_1,0,P_1,0}\exp[i(\boldsymbol{p}+\boldsymbol{P})\cdot\boldsymbol{r}]\right.$$

$$\left.+a^*_{p_1,0,P_1,0}\exp[-i(\boldsymbol{p}+\boldsymbol{P})\cdot\boldsymbol{r}]\right\}$$

$$+\sum_{p_2+P_2>0}\left\{a_{\boldsymbol{p},\boldsymbol{P}}\exp[i(\boldsymbol{p}+\boldsymbol{P})\cdot\boldsymbol{r}]\right.$$

$$\left.+a^*_{\boldsymbol{p},\boldsymbol{P}}\exp[-i(\boldsymbol{p}+\boldsymbol{P})\cdot\boldsymbol{r}]\right\}$$

The detail definition of Eq. (2.2.15) to Eq. (2.2.15) are shown in Appendix A.

2.3 Disorder parameter ζ of Li and Nattermann

M. S. Li and T. Nattermann([26] T. Natterman) defined the dimensionless parameter ζ to control the relative disorder strength, and expand the random Gaussian disorder in renormalized Hermite polynomials to express the disorder term of GL free energy equation. The disorder term of M. S. Li and T. Nattermann is

$$\int d^2r\ \alpha\delta T_c(r)|\psi|^2 \tag{2.3.1}$$

here $\delta T_c(r)$ is real and Gaussian distributed with

$$\overline{\delta \mathrm{T}_c(r)} = 0 \tag{2.3.2}$$

$$\overline{\delta \mathrm{T}_c(r)\delta T_c(r')} = \zeta^2 T_c^2 \xi^{-2} \delta_{\xi}(r - r') \tag{2.3.4}$$

They defined the disorder parameter with following relation

$$\tilde{\zeta} = \frac{\zeta b^{\frac{1}{2}}}{\pi^{\frac{1}{2}}(1 - t - b)} \tag{2.3.5}$$

Connecting our disorder term with their notation, we have

$$\frac{Rl\alpha T_c(1-t)}{8\pi L^2(\pi b' T)^{\frac{1}{2}}} = \frac{l^2 a_T^2 \tilde{\zeta}^2}{64\pi^2 L^2} \tag{2.3.6}$$

By controlling the specific $\tilde{\zeta}$ to generate the corresponding complex random fields, we can get various degree disorder vortex systems.

2.4 MC simulation method.

Metropolis algorithm:

The standard Monte Carlo method with Metropolis algorithm ([28] D. P. Landau and K. Binder; [27] Y. Kato) was used to simulate the two-dimensional pure and disordered vortex system. In the classic Metropolis method, we use a transition probability which depends on the difference of energy $\Delta \mathrm{E}$ between the initial and trial configuration to determine whether the trial configuration is accepted or not. Now I introduce the Monte Carlo method as follows. First, we choose an initial configuration and calculate the initial energy E_m. Second, we choose a site $\mathrm{C}_j \in C^N$ randomly and generate the trial configuration with C_j^{new} by using the rule: $\mathrm{C}_j^{new} \to \mathrm{C}_j^{old} + \epsilon \Delta \mathrm{C}$, where $\Delta \mathrm{C}$ is a complex number which is chosen randomly from the region $|\mathrm{Re}\Delta \mathrm{C}| \leq 1$ and $|\mathrm{Im}\Delta \mathrm{C}| \leq 1$ in the complex plane. Third, we calculate the energy E_n of trial configuration and the difference of energy $\Delta \mathrm{E}$, here $\Delta \mathrm{E} = \mathrm{E}_n - \mathrm{E}_m$. If $\Delta \mathrm{E} \leq 0$, the system accepted the trial configuration, but if $\Delta \mathrm{E} \geq 0$, the trial configuration is accepted with a probability $\exp(-\beta \mathrm{E})$. Generating a random number γ uniformly in the interval $[0,1]$, if $\gamma \leq \exp(-\beta \mathrm{E})$ the trial configuration is accepted, otherwise it is rejected. This process is called Monte Carlo step/site (MCS/site). Note that the old configuration is still counted again for averaging if the trial configuration is rejected. By using Monte Carlo method, the system will fall into the stable states and reach the equilibration, and the characteristics of vortex system can be measured.

Monte Carlo calculations:

We used

$$\mathrm{C}_{l_1,l_2}^{new} = \mathrm{C}_{l_1,l_2}^{old} + \delta_{l_1-j_1}\delta_{l_2-j_2}\Delta \tag{2.4.1}$$

to vary the value of a specific wave function coefficient C_j in our Monte Carlo simulation, here $\Delta = \epsilon\Delta\mathrm{C}$. Note that j and l are vectors which composed of two reciprocal vectors $\tilde{\mathrm{d}}_1$ and $\tilde{\mathrm{d}}_2$. Furthermore we used these equation to calculate the energy of trial configuration and only discussed the changes of the summation of wave function coefficient product, the detail of Monte Carlo calculations are worked out in Appendix C. The summation of wave function coefficient product of trial configuration is

$$\begin{aligned}\sum_{l_1,l_2} \mathrm{C}_{l_1,l_2}^{new*}\mathrm{C}_{l_1,l_2}^{new} &= \sum_{l_1,l_2} \left(\mathrm{C}_{l_1,l_2}^{old} + \delta_{l_1-j_1}\delta_{l_2-j_2}\Delta\right)^* \left(\mathrm{C}_{l_1,l_2}^{old} + \delta_{l_1-j_1}\delta_{l_2-j_2}\Delta\right) \\ &= \sum_{l_1,l_2} \left(\mathrm{C}_{l_1,l_2}^{old}\mathrm{C}_{l_1,l_2}^{old*} + \delta_{l_1-j_1}\delta_{l_2-j_2}\mathrm{C}_{l_1,l_2}^{old*}\Delta + \delta_{l_1-j_1}\delta_{l_2-j_2}\mathrm{C}_{l_1,l_2}^{old}\Delta^* + \Delta\Delta^*\right) \\ &= \mathrm{C}_{l_1,l_2}^{old*}\Delta + \mathrm{C}_{l_1,l_2}^{old}\Delta^* + \Delta\Delta^* + \sum_{l_1,l_2} \mathrm{C}_{l_1,l_2}^{old*}\mathrm{C}_{l_1,l_2}^{old}\end{aligned} \tag{2.4.2}$$

Evidently the $\sum_{l_1,l_2} \mathrm{C}_{l_1,l_2}^{old*}\mathrm{C}_{l_1,l_2}^{old}$ term can be calculated directly by old configuration, hence we can store it to simulate the vortex system more efficiently. The old calculation results always can be applied in new one and a lot of computer time is saved, the CPU time in one Monte Carlo step $\propto \mathrm{L}^2$. There are 16×16 numbers of vortices in our simulation. We took 6×10^6 MC steps to reach the thermal equilibration and calculated the physical quantities over $1 \times 10^6 \sim 1 \times 10^7$ MC steps.

The physical quantities were measured every $30 \sim 50$ MC steps. We control ϵ in a reasonable region to make the acceptance ratio is $0.3 \sim 0.4$ and then the vortex system reach the thermal equilibrium state efficiently. All the simulations were started from the heating processes with the initial configuration which is defined as follows: $C_i = \sqrt{\frac{|a_T|}{\beta_A}}$, here C_i is one of all coefficients of wave function and others are equal to zero, $\bar{\beta}_A \sim 1.16$ is the mean-field value of the Abrikosove ratio.

Chapter 3

Indicators of the four vortex phases and the MC data Analysis

3.1 Vortices configuration

Fig. 3-1-1 are the snapshots of the spatial distribution of the order-parameter field $|\psi(x,y)|^2$ for $a_T < t_m$ and $a_T > t_m$, respectively. There are $16 \times 16 = 256$ vortices in each sample and we used 6×10^6 Monte Carlo steps to make sure the system reaches the equilibration by referring the MC simulation by Y. Kato and N. Nagaosa ([27] Y. Kato). The melting temperature was calculated of the sample with finite size,

$$t_m = -13.02 \text{ for } N_s = 256 \tag{3.1.1}$$

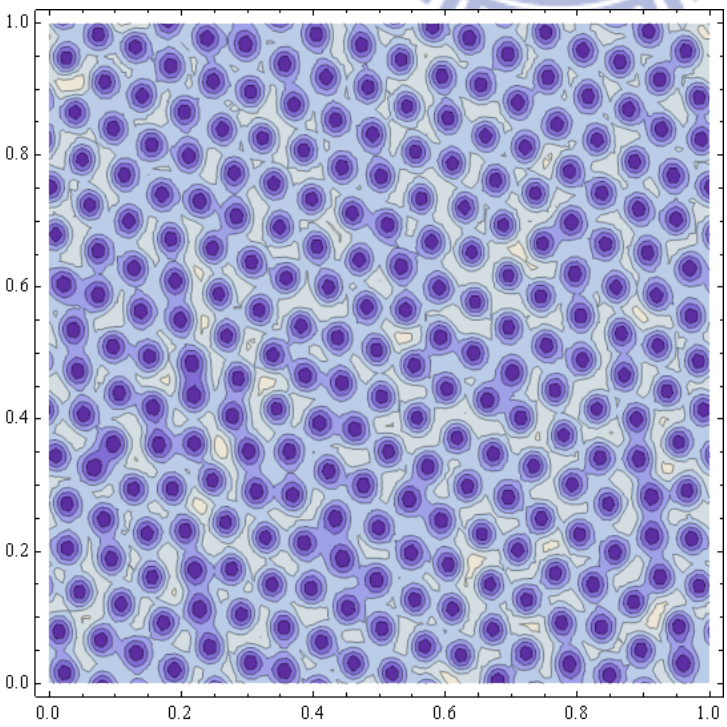

Fig. 3-1-1(a): snapshots of the spatial distribution of the order-parameter field $|\psi(x,y)|^2$ for $a_T < t_m$.

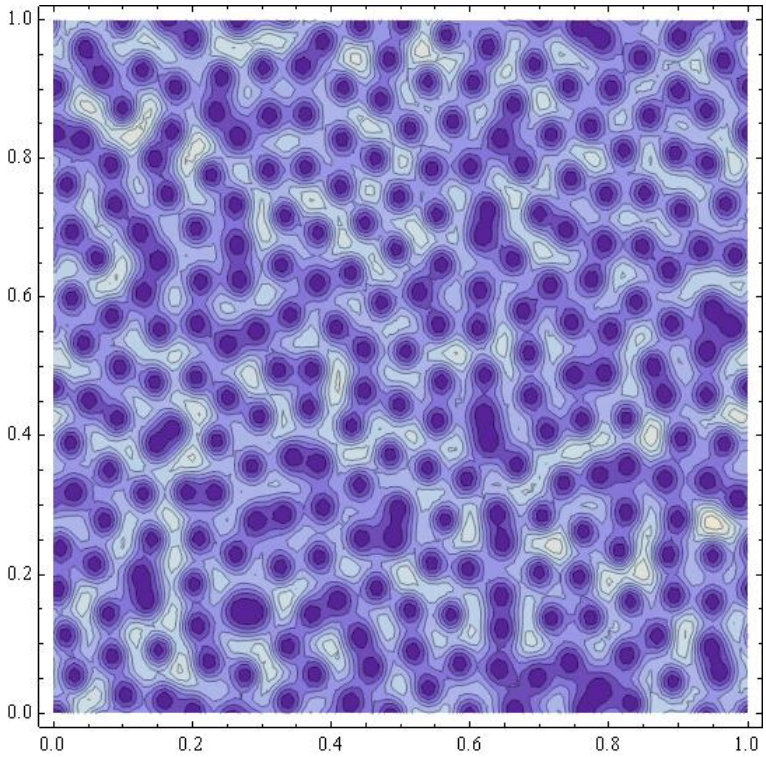

Fig. 3-1-1(b): snapshots of the spatial distribution of the order-parameter field $|\psi(x,y)|^2$ for $a_T > t_m$.

One can easily see that the vortices arrayed regular and randomly for $a_T < t_m$ and $a_T > t_m$ in Fig. 3-1-1. The Fourier transform of Fig. 3-1-1 is shown in Fig. 3-1-2. One can find a big change while the pattern is structure less above t_m and the pattern below t_m shows the six sharp peaks with hexagonal symmetry indicating the existence of the lattice of the vortices. I try to analysis the change of the Fourier transform pattern for disorder parameter ζ and reduced temperature a_T due to $\zeta = 0 \sim 1$ and $a_T = -17 \sim -11$ to find the phase transition.

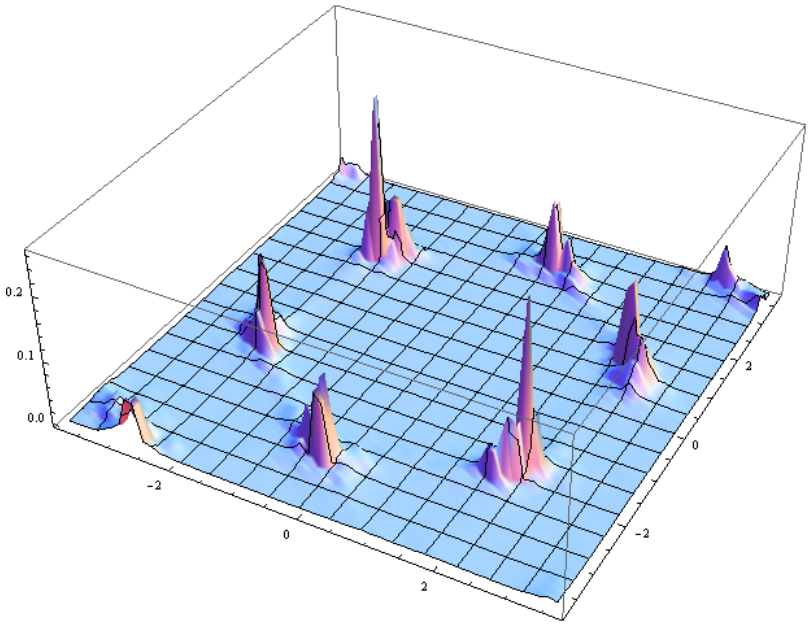

Fig. 3-1-2(a): The Fourier transform of Fig. 3-1-1(a).

One can see beautiful hexagonal lattice

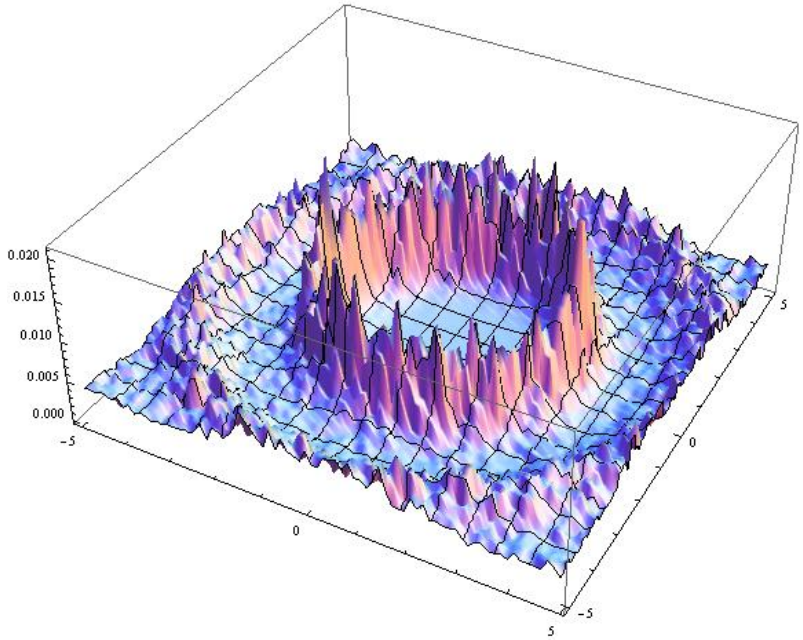

Fig. 3-1-2(b): The Fourier transform of Fig. 3-1-1(b).

It’s a structure less pattern instead of beautiful hexagonal lattice

3.2 Rotation average

We made discrete data with reduced temperature $a_T = -17 \sim -11$ and reduced disorder $\zeta = 0 \sim 1$ which are snapshots in the equilibrium state. There are 20 samples with each a_T and ζ. The first thing we need to do is averaging the 20 samples of the Fourier transform pattern. Since they are just snapshots in equilibrium state, averaging them let us get rid of the extreme un-objective sample so that we can mark the phases correctly. Consider the patterns with beautiful lattice for $a_T < t_m$ first. I rotated the highest peak of the first ring to the same angle and averaged them so the information of the patterns will not lose in averaging directly. It's no doubt that the other peaks will be moved to the same coordinate because it's always a hexagonal lattice at first ring. And I averaged the six peaks to eliminate the height difference between the peaks because I don't want to always see a peak much taller than others due to I made it in the rotation. Fig. 3-2-1 is the simple interpretation of the rotation. Comparing the patterns before and after rotation averaging, one should find they are the same since it is structure less originally and they have a big difference since it is a hexagonal lattice originally. Fig. 3-2-2 shows the series procedure of the rotation averaging.

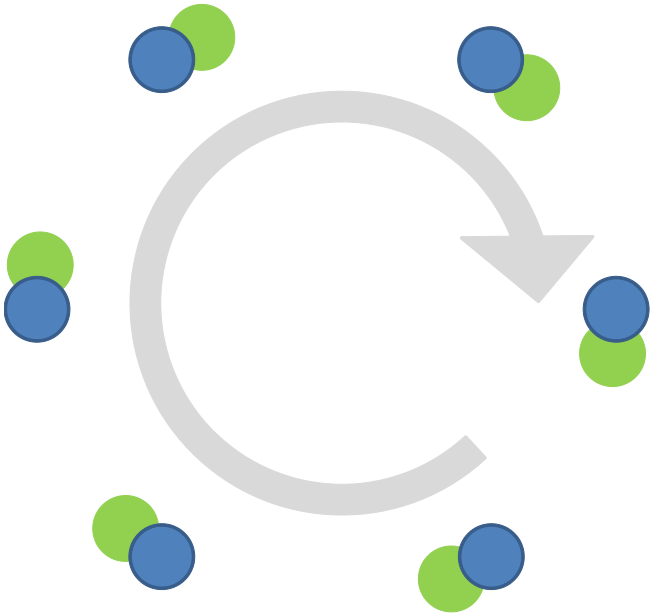

Fig. 3-2-1: Interpretation of the rotation: I rotated all the peaks to the same position.

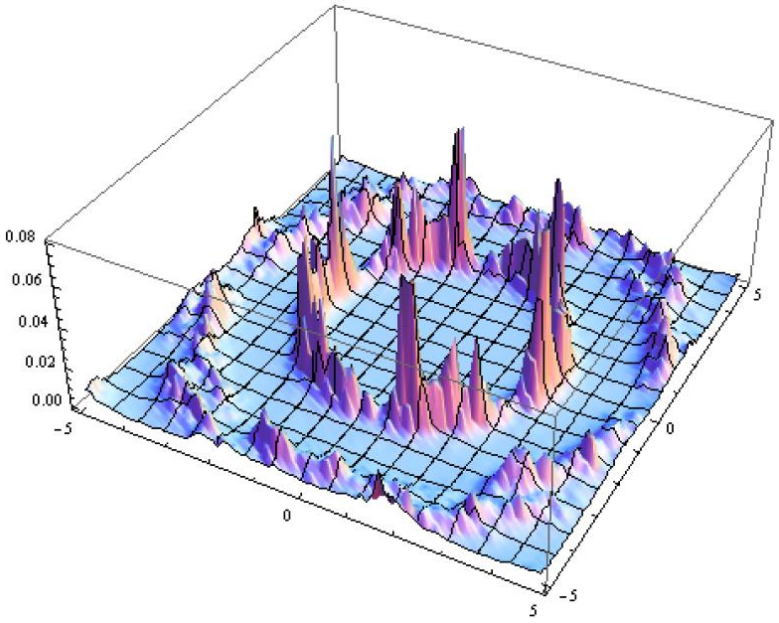

Fig. 3-2-2(a): The pattern of vortices averaged directly. One will get averaged patterns like this with any reduced temperature and disorder without rotation.

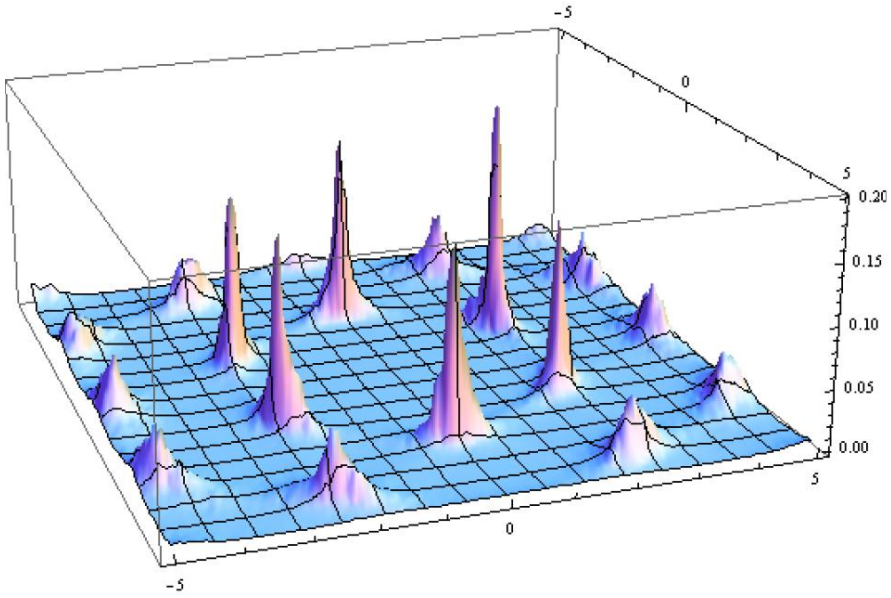

Fig. 3-2-2(b): There is a tallest peak much taller than others due to that I choose the highest peak rotating to the same position.

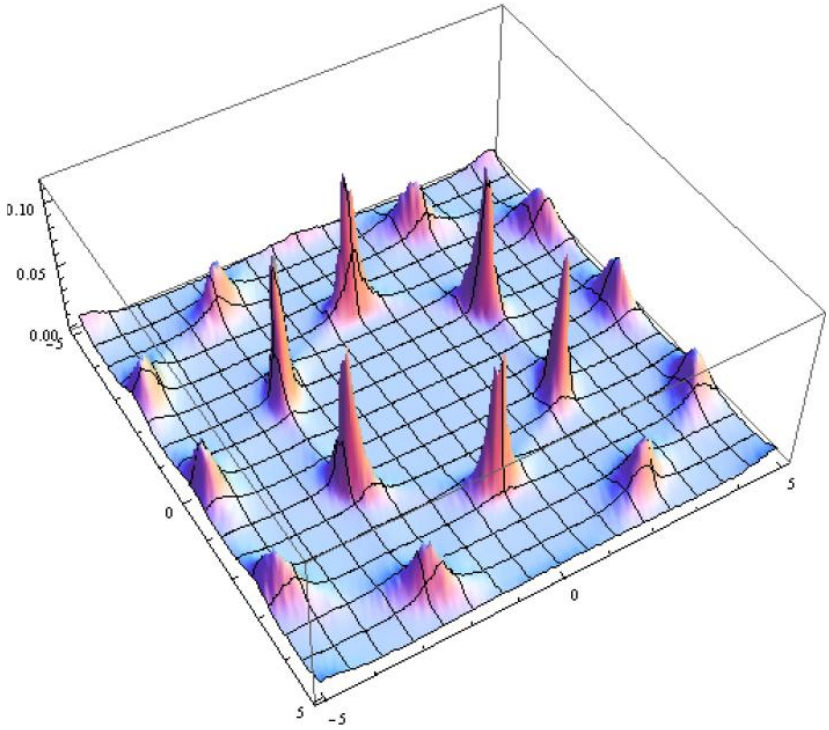

Fig. 3-2-2(c): After angle averaging: averaged six parts of dividing by every 60 degrees to eliminate the un-objective peak.

I concluded the trend of the patterns changing. As the temperature increasing, the vorteice melted by thermal fluctuation. And as the disorder increasing, the vortices approach pinning on the disorder and also destruct the lattice. Fig. 3-2-3 and Fig. 3-2-4 show the changing with reduced temperature and reduced disorder.

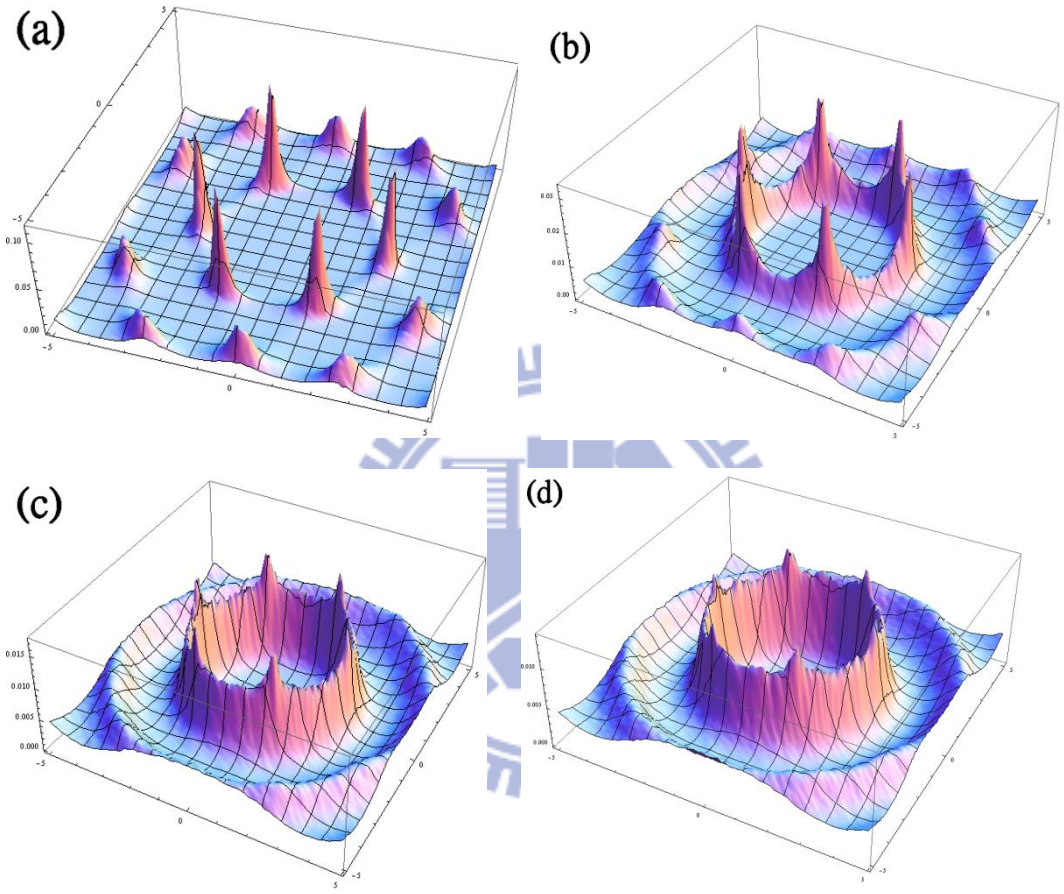

Fig. 3-2-3: Series Fourier transform pattern, the temperature getting higher from (a) to (d).

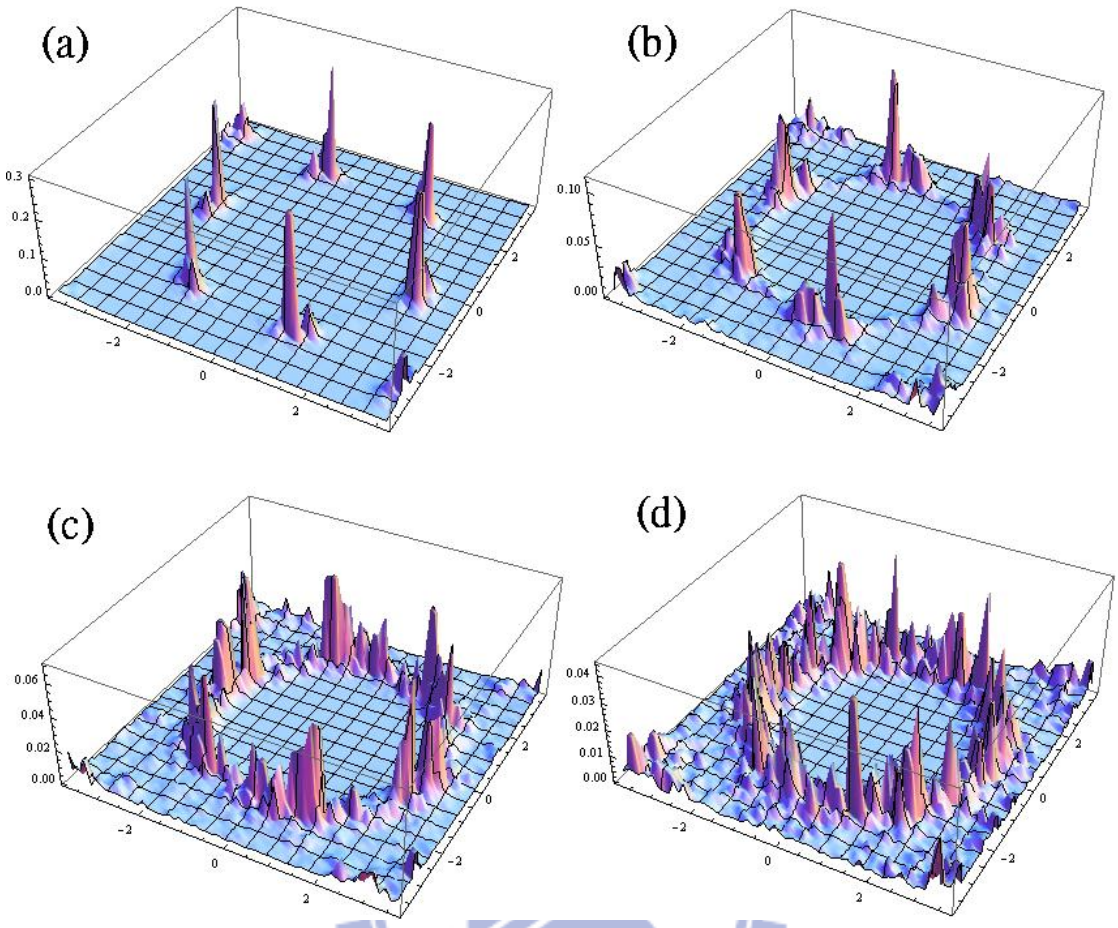

Fig. 3-2-4: Series Fourier transform pattern, the disorder getting higher from (a) to (d).

According to the appearance of the samples after averaging, I marked the phase diagram to three parts: the Fourier transform pattern with (a)beautiful hexagonal lattice, (b)structure less lattice and (c)disturbed but still looked like hexagonal lattice that show on Fig. 3-2-5. But it's difficult to separate the phases precisely so I tried some numerical analysis that I introduce in the following section.

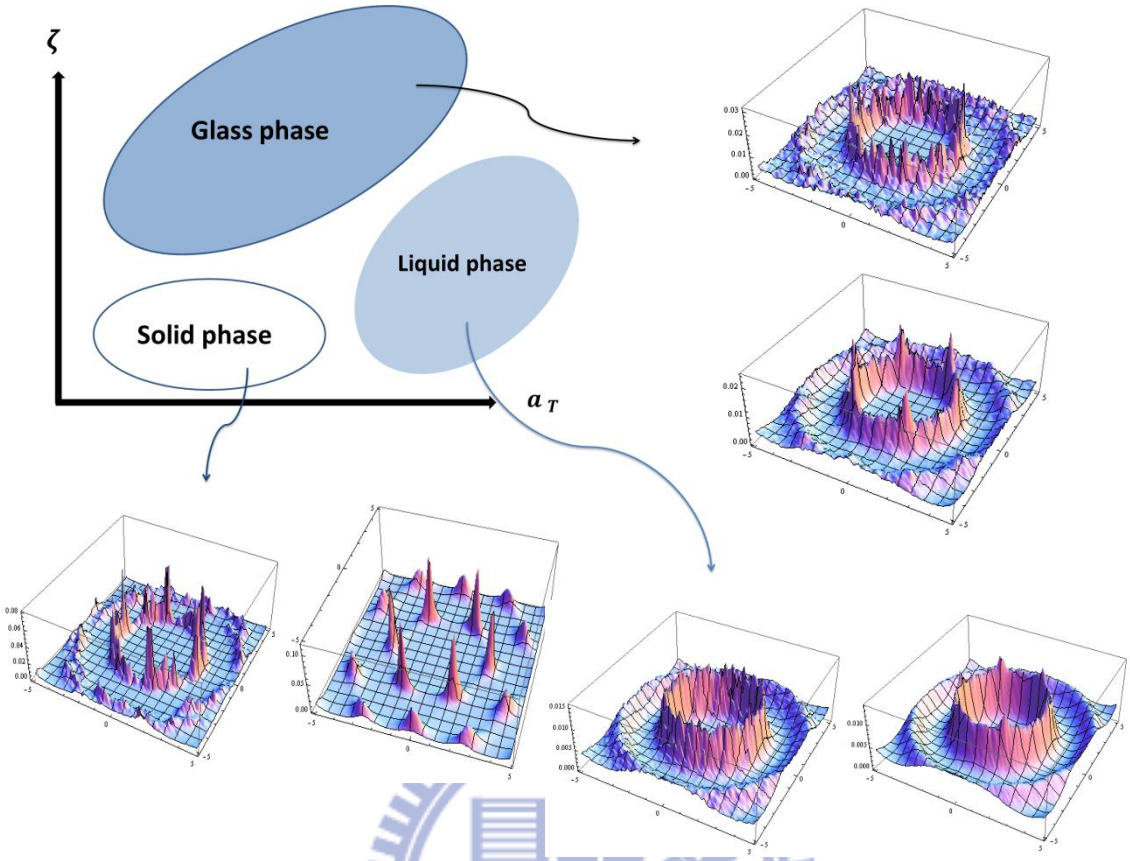

Fig. 3-2-5: The phase diagram can be separate to three parts roughly. In solid phase, there are six sharp peaks separately formed the beautiful hexagonal lattice. While in vortex liquid phase, there's nearly no peak observed in the diagram so looked like a smooth ring. And one can see the vortices "sticky" connected by each other in the glass phase.

3.3 Indicator of melting line

To determine the melting line precisely, we need a numerical analysis. I integrated the first ring and the six peaks individually as shown in Fig. 3-3-1. By comparing the integration of each individual peaks and the first ring

$$\frac{\int integral[peaks]}{\int integral[ring]} \equiv R_m \tag{3.3.1}$$

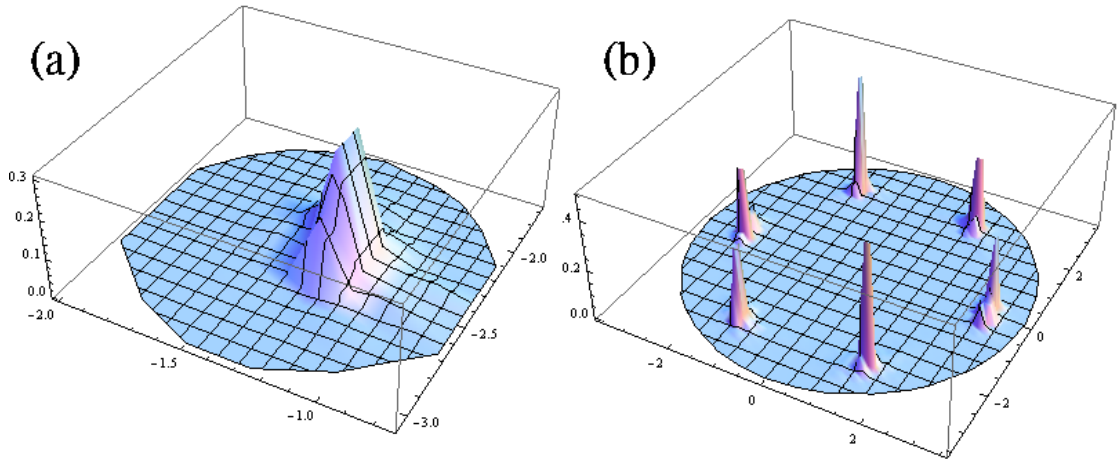

Fig. 3-3-1: Interpretation of R: (a) is enlarged pictures of a single peaks, (b) is the snapshot including the first ring only.

In theoretical prediction, there's almost no difference between these two integral in solid. So I expected there's a big step at the melting line. First I choose the highest point in the first ring, and summed over the value of nearby points. The other five peaks are determined by choosing the five peaks having a included angle respond to origin and the highest point in 60, 120, 180, 260 and 320 degrees. For ideal solid phase the ratio R_m must be 1. And the ratio for ideal liquid is about 0.42 that I tested it by a simulation of ideal liquid as Fig. 3-3-2.

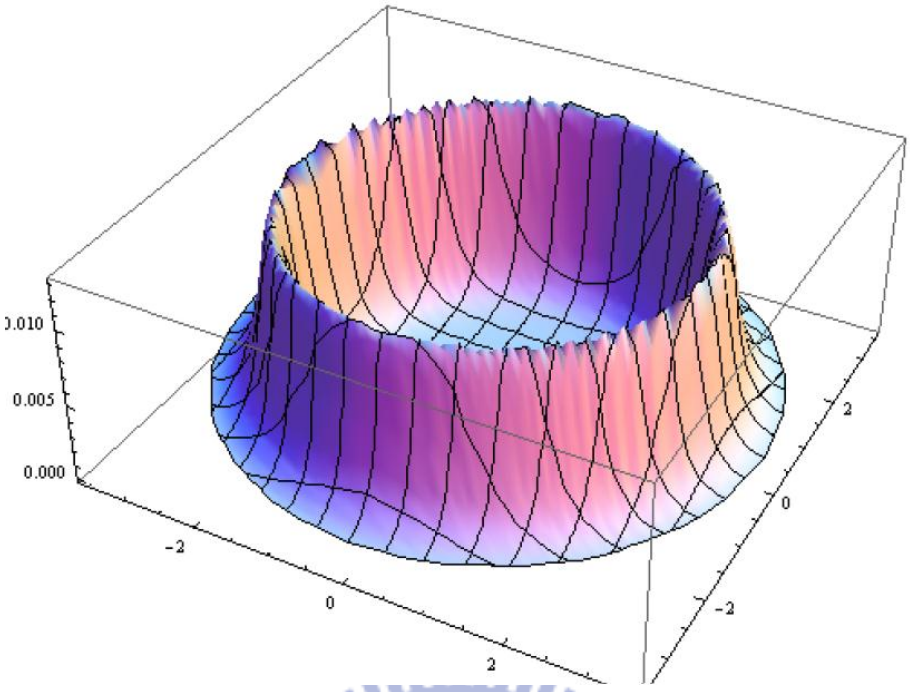

Fig. 3-3-2: Ideal liquid Fourier transform of $|\psi|^2$

3.4 Indicator of glass (irreversibility) line

To determine the glass line precisely, we need to compare the vortices position in two different initial conditions. If the system is in Brrag glass phase or vortex glass phase. The vortices will prefer pinning on the disorder. So I rotated the highest votex peak of the first ring to the same position with two different initial conditions like I did in the average. And I multiplied these two plots and integrated it. Before integrating, I had eliminated the points value nearby the highest point included the highest point to avoid always getting high integral value nearby the highest point. If the system isn't in glass phases the peaks with two initial conditions will be in almost the same position, and the integral must be much larger than the integral with

system in glass phases. The precede work before the integration show in Fig. 3-4-1. For convenient, I call the integration as I_g.

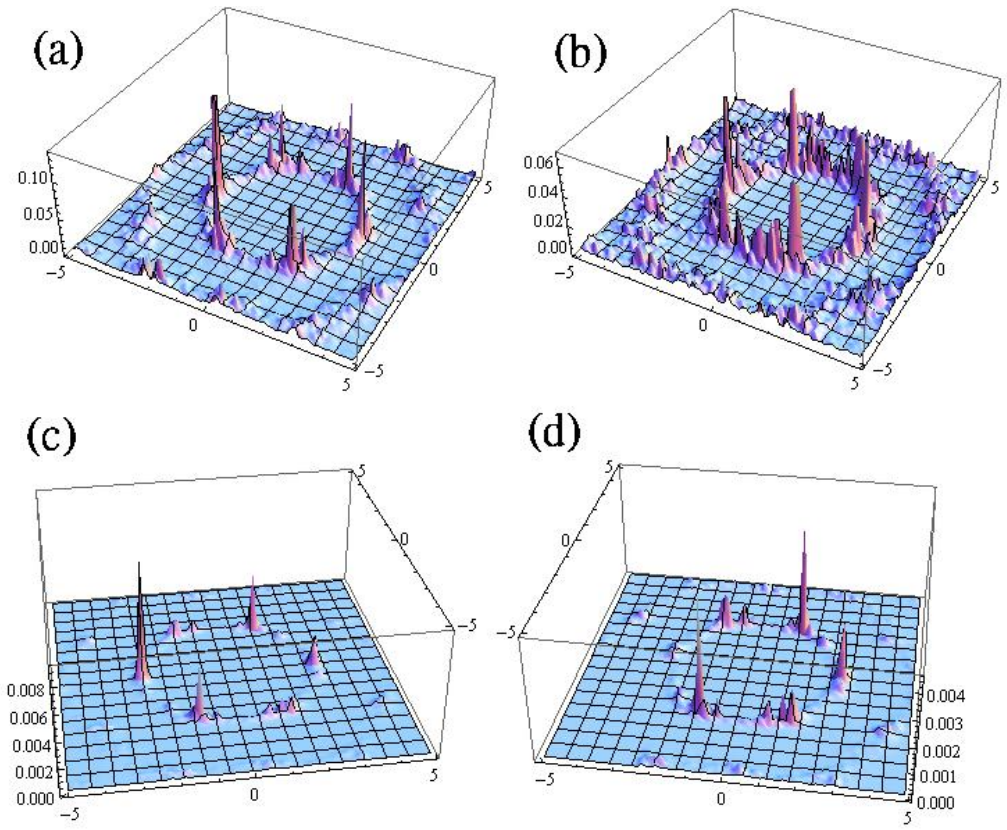

Fig. 3-4-1: The precede work before the integration: (a) vortices with random distribution disorder; (b) vortices with lattice distribution disorder; (c) after multiplied of (a) and (b); (d) the highest peak is eliminated.

Chapter 4

The phase diagram of the vortex matter

4.1 Melting line

Using the indicator defined in section 3.3, I sketched the $a_T - \mathrm{R}_m$ diagram of the pure system in two initial conditions (In ideal cases, there's no difference between two systems with random distribution of disorder and lattice like distribution of disorder.)(Fig. 4-1-1). From Fig. 4-1-1 we can see that the boundary value of solid and liquid phase is about 0.5. If the value of R_m is above 0.5, I said the system is more like in solid phase. Otherwise, if R_m is below 0.5, the system is more like in liquid phase.

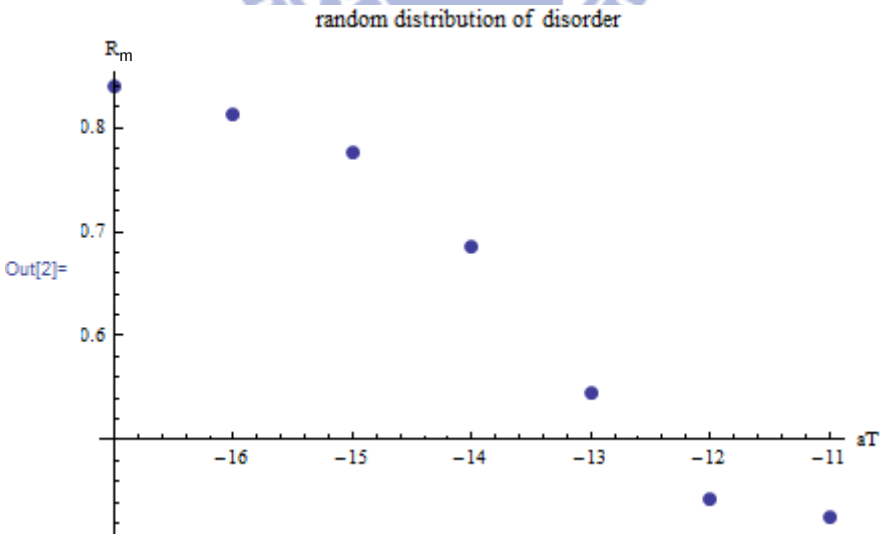

Fig. 4-1-1(a): $a_T - \mathrm{R}_m$ diagram with random distribution of disorder in pure system.

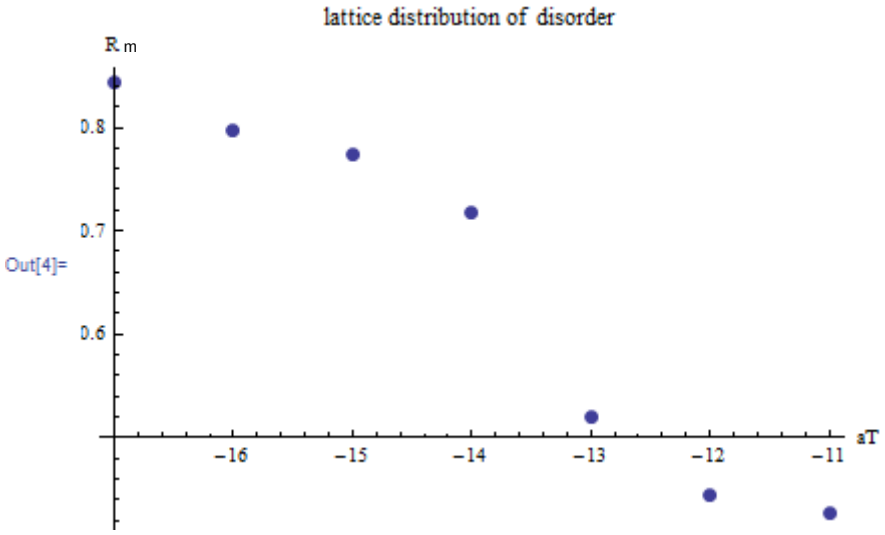

Fig. 4-1-1(b): $a_T - \mathrm{R}_m$ diagram with lattice distribution of disorder in pure system.

Use $\mathrm{R}_m = 0.5$ to be the indicator of the boudary of solid phase and liquid phase. I calculated the ratio R_m of each samples with reduced temperature during $a_T = -17 \sim -11$ and disorder parameter during $\zeta = 0 \sim 1$. As shown in Fig. 4-1-2, it's clear to see the melting line in the $a_T - \zeta$ diagram. It matches the melting line of the contour plot of $a_T - \zeta$ diagram that one can find the transition line at the same position (Fig. 4-1-3).

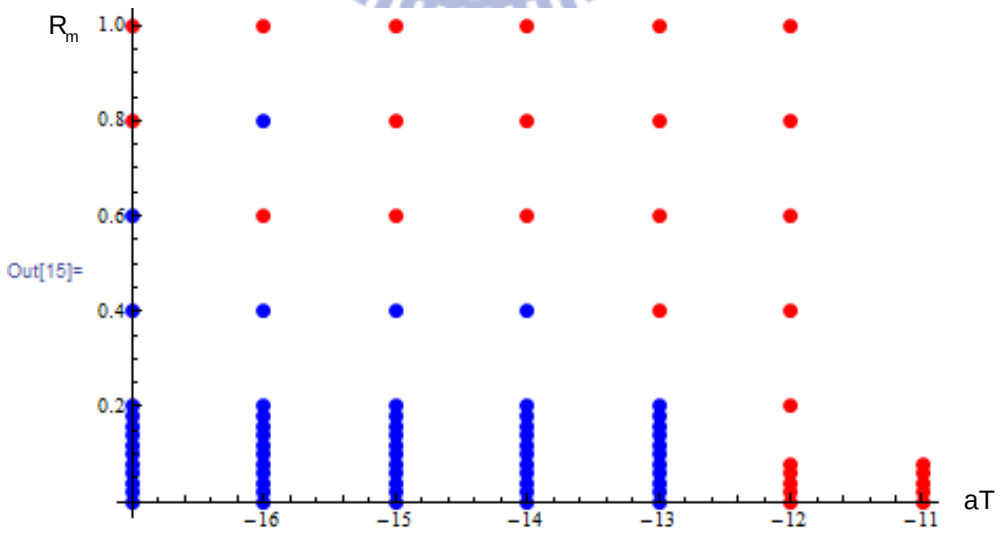

Fig. 4-1-2(a): If the ratio R of the system is larger than 0.5, it marked red point. In another way, if the ratio R of the system is smaller than 0.5, it marked blue point. It's the statistical of R with random distribution initial condition.

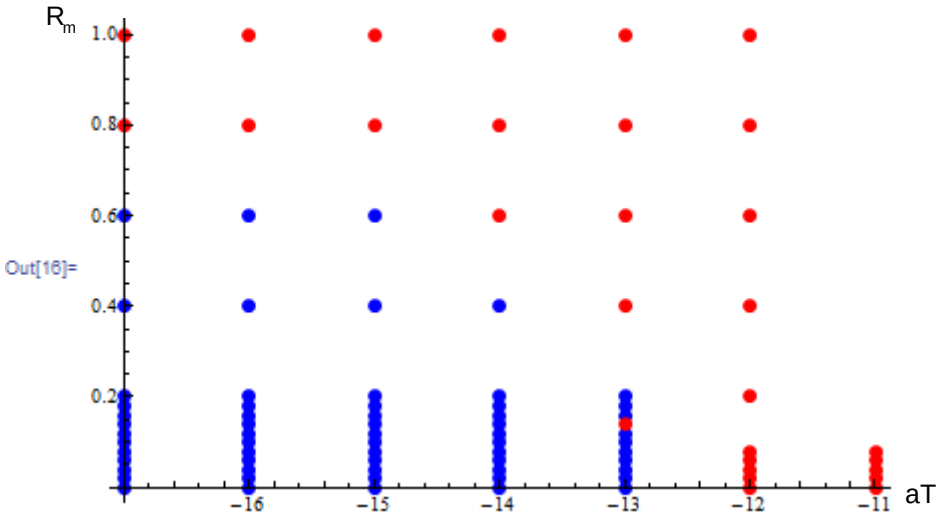

Fig. 4-1-2(b): It's the statistical of R with lattice-like distribution initial condition. One can see the same melting line clearly both in random distribution i.c. or in lattice-like distribution i.c..

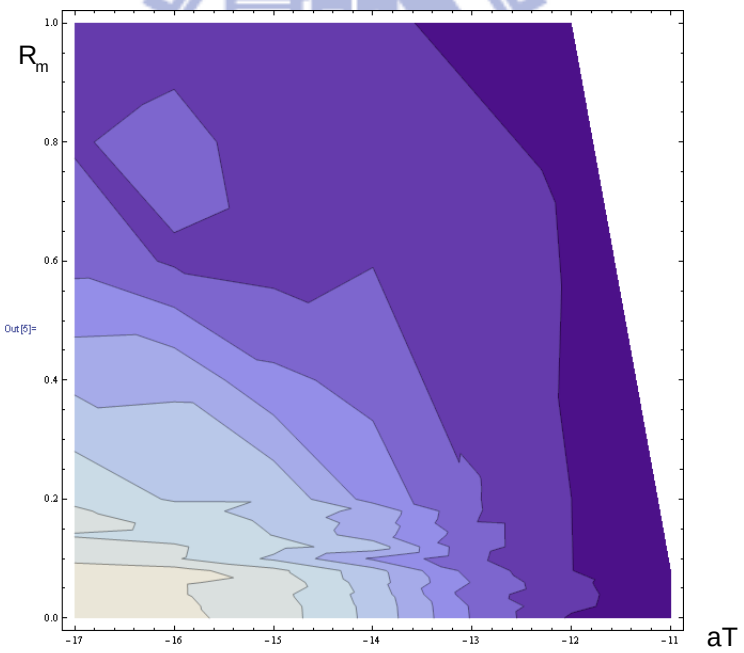

Fig. 4-1-3(a): Contour plot of $a_T - \zeta$ diagram of R_m with random distribution disorder

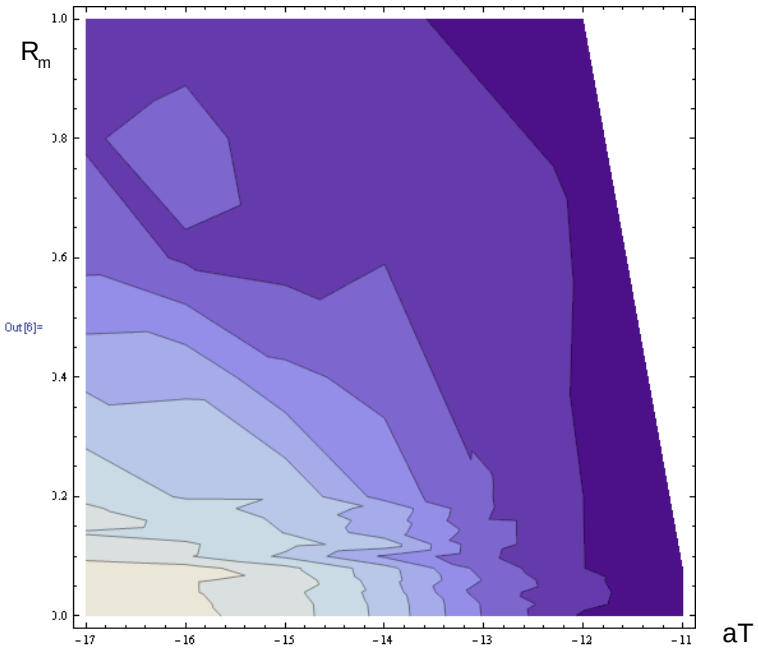

Fig. 4-1-3(b): Contour plot of $a_T - \zeta$ diagram of R_m with lattice like distribution disorder. one can see the transition line is the same with two different distribution of disorder by comparing (a) and (b), and fitted the transition line in Fig. 4-1-2.

4.2 Glass (irreversibility) line

Using the indicator defined in section 3.4 and sketched the $a_T - I_g$ diagram directly without considering the thermal fluctuation is strong at high temperature, we got a glass line isn't objective (Fig. 4-2-1) that the glass point should be higher as the temperature getting higher because the peak is hard to pin on the disorder by the strong thermal fluctuation at high temperature. The reason to see a un-objective trend is because the vortices almost melted at high temperature, so of course the integral I_g is smaller than the vortices integral under low temperature (no sharp

peaks).

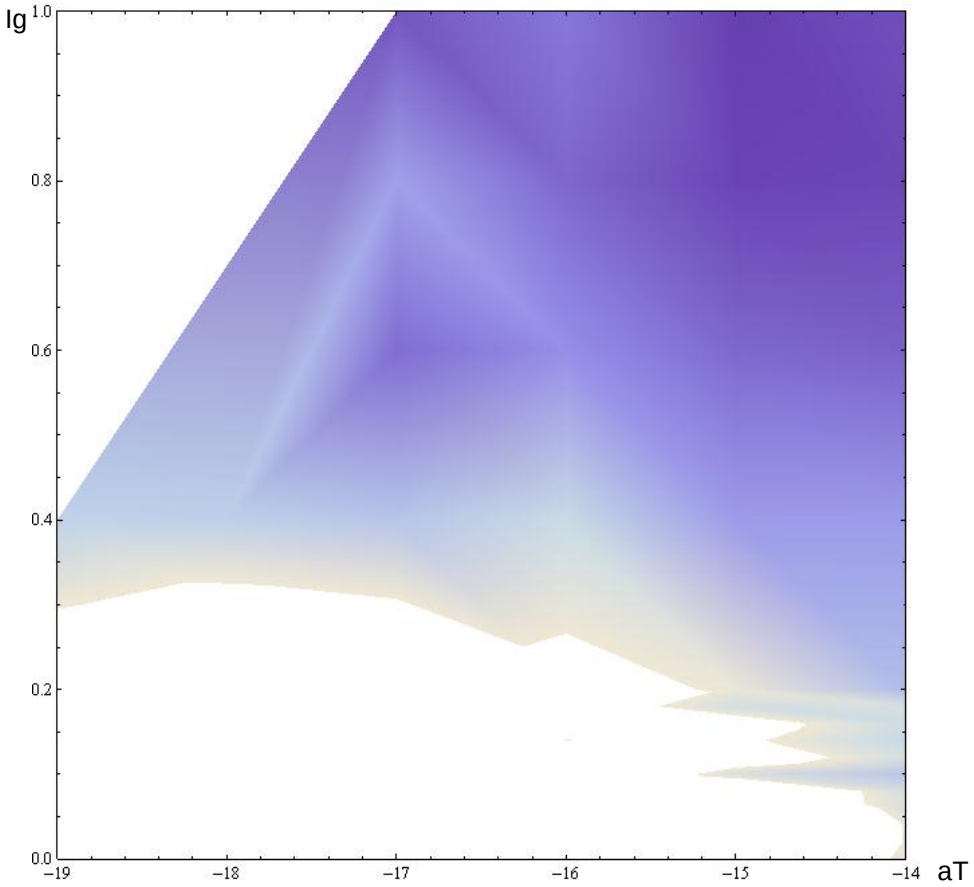

Fig. 4-2-1: Density plot without correction, one can see the integration I getting higher as temperature getting higher at low temperature but getting lower as temperature getting up.

Here are two ways to solve the problem. One is see the plot fixed one temperature at a time. The border on the step is the transition point of the glass line (Fig. 4-2-2). By observing the plot fixed one temperature at a time, one will not confused by the number but focuses on the variation of I_g. Another way to see the trend of glass line is dividing the integral value I_g of disordered system by the integral I_g^{pure} of pure system. In ideal case, vortices with two different initial condition in pure system map to each other perfectly and the integral is always larger

than the case in disorder system. So it's reasonable to divided the integral value of disorder by the integral of pure system to "normalize" the integral values. We can see the trend in the contour plot after correction by the second way in Fig. 4-2-3 that it fit the transition points in Fig. 4-2-3 with different a_T.

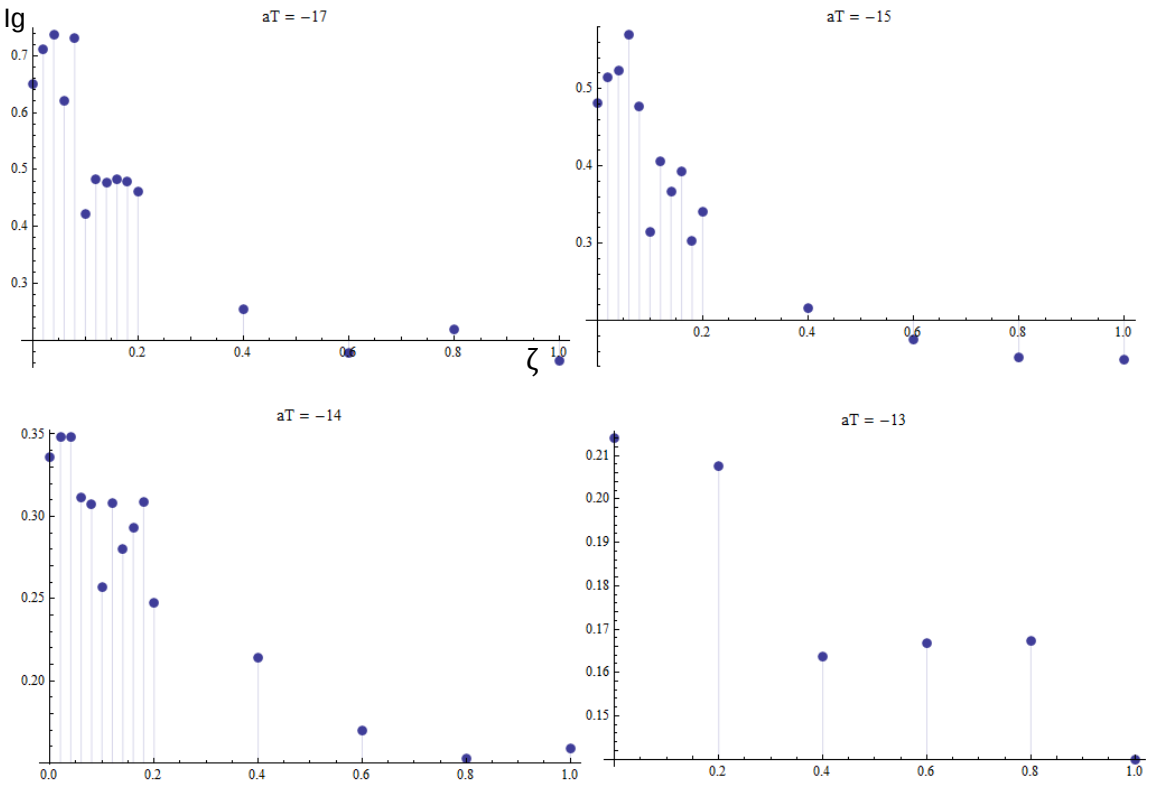

Fig. 4-2-2: $\zeta - I_g$ diagram with fixed a_T at a time. The decrease speed as disorder getting larger of I_g is slow down at high temperature. It means it's hard to pin on the disorder at high temperature so there's no big difference between low ζ and high ζ.

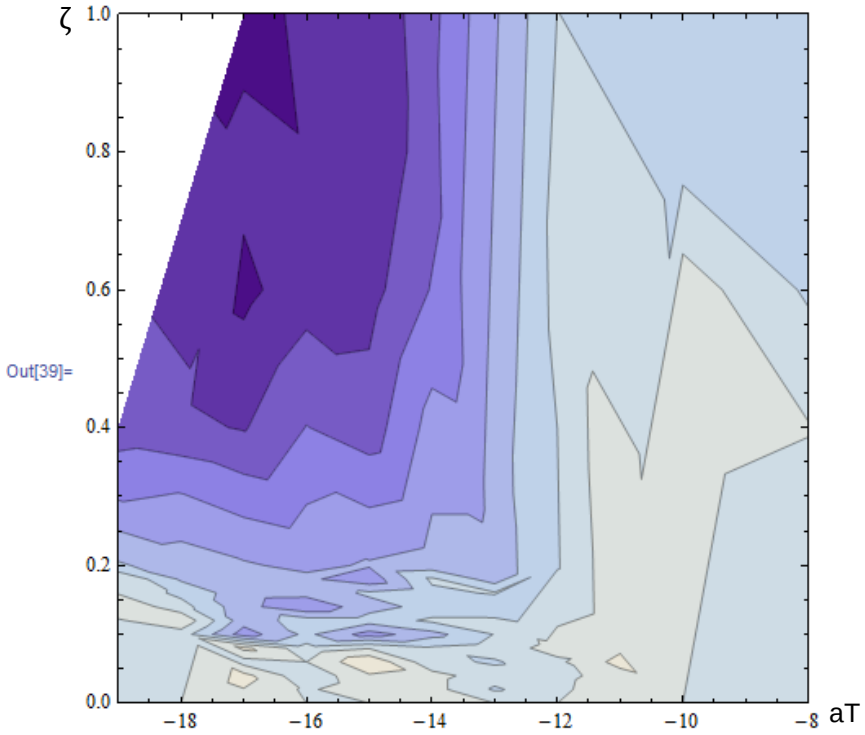

Fig. 4-2-3: Contour plot after correction. One can see the integration I_g getting higher sharply at $a_T = -13$.

4.3 Phase diagram

Assemble the results in section 4.1 and 4.2. I got a $a_T - I_g$ phase diagram roughly showed in Fig. 4-3-1. The melting point of my analysis in pure system is at $a_T = -13$ approximately. It's the same as the calculation by Kato ([27] Y. Kato) in MC simulation with finite sample. The trend of melting line as disorder getting large fit the theory prediction that the melting point with larger disorder is at lower temperature. Because the well accuracy of melting line, the glass line in my analysis is reliable. From my analysis, the Abrikosov lattice is existence. There is no pinning effect since the disorder is weak. From Fig. 4-2-2 one can see there is a big step when

the disorder get strong enough. Also from the big difference of patterns of the Fourier transform of $|\psi|^2$ between solid phase (Abrikosov phase) and glass phase (Brag glass or vortex glass) we saw in Fig. 3-2-4, the Abrikosov lattice is existence indeed.

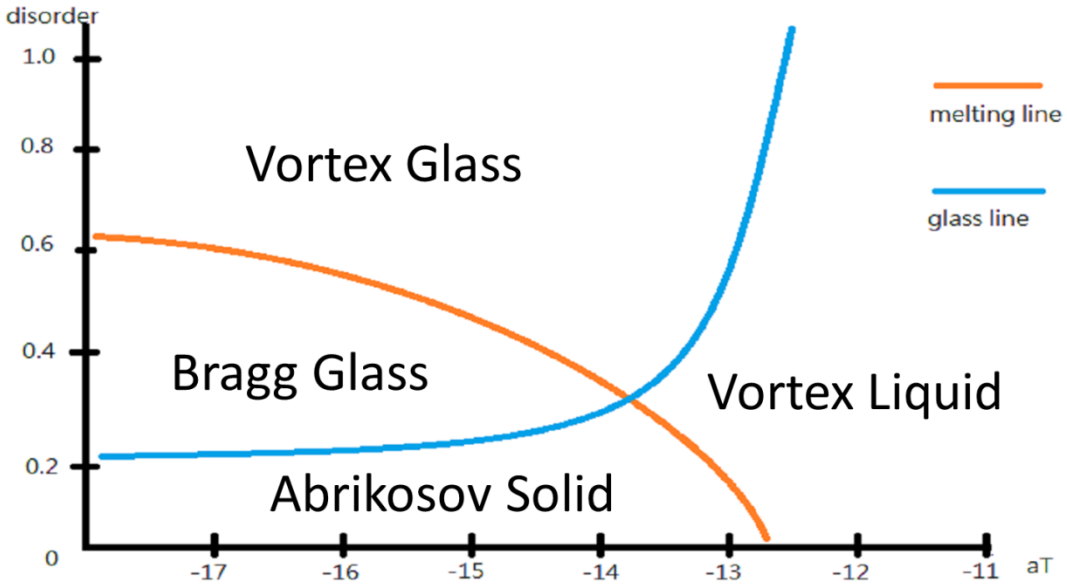

Fig. 4-3-1: $a_T - \zeta$ phase diagram. The blue line is the glass transition line; The red line is the melting transition line.

Chapter 5

Conclusion

The vortex simulation in highly anisotropic layered type II superconductors has been studied by Monte Carlo simulation in two dimensional Ginzburg-Landau model with the quasi-momentum basis. Vortices structure are studied with disorder parameter $\zeta = 0 \sim 1$ and reduced temperature $a_T = -17 \sim -11$ in the thesis. I developed the rotation averaging to analysis the snapshots of the Fourier transform of the superfluid density. Using the rotation averaging, I compared the diagrams of the average of samples with each disorder parameter and reduced temperature before and after rotation to classify the diagrams into three categories: Abrikosov lattice phases, vortex liquid phase and glass phase. In solid phase (Abrikosov phase), there are six sharp peaks separately formed the beautiful hexagonal lattice. While in vortex liquid phase, there's nearly no peak observed in the diagram so looked like a smooth ring. And one can see the vortices "sticky" connected by each other in the glass phase. To identify the transition line precisely, I made two indicators for melting line and glass line as R_m and I_g to analysis phase diagram numerically. R_m is defined by the compare of the integral of finite area near ideal solid peaks and the integral of the first ring (the central lattice). R_m must be 1 in ideal solid phase since all contribution of the integral of the first ring comes from the six sharp peaks only. In another way, R_m must be small because most contribution of the integral of the first ring doesn't come from the area near the peaks even there's no peaks in the

liquid phase. The glass transition line indicator I_g is defined by the multiplication of the samples at the same disorder parameter and reduced temperature but with two different distribution of disorder. There's no pinning effect in the ideal Abrikosov phase so the Fourier transform distribution of the samples with two different distribution of disorder are the same. So one will get a high value of I_g, since the samples of two kind distributions of disorder map on each other almost perfectly. As the system get into the glass phase, there is stronger pinning effect as the disorder getting larger. So the samples of two kind distributions of disorder didn't map on each other except the peak I rotated it to the same position. I got the phase diagram by these two indicator that the melting line coincide with many experiments. That makes the glass (irreversibility) line of the analysis reliable. The glass (irreversibility) line in the analysis confirm with the theory prediction. Here I offer a reliable $a_T - \zeta$ diagram in the present.

Appendix

Appendix A

The quadratic term of GL function is

$$\rho(x,y) = |\psi(x,y)|^2 = \sum_{\boldsymbol{k},\boldsymbol{l}} C_{\boldsymbol{k}}^* C_{\boldsymbol{l}}\, \varphi_{\boldsymbol{k}}^* \varphi_{\boldsymbol{l}}\,, \tag{A.1}$$

we substitute the form of the quasi-momentum

$$\varphi_k = exp\{-ixk_x\}\varphi_0\big(x - k_y, y + k_x\big)\,, \tag{A.2}$$

into the basic formula as

$$\varphi(r)\varphi_{\boldsymbol{k}}^*(r) = \sum_{Q_1\tilde{d}_1+Q_2\tilde{d}_2} exp[i(\boldsymbol{k}+\boldsymbol{Q})\cdot\boldsymbol{r}]exp\left[\frac{\pi i}{2}(Q_1^2+Q_1)\right]exp\left[-\frac{(\boldsymbol{k}+\boldsymbol{Q})^2}{4}\right.$$
$$\left.-\frac{i(k_x+Q_x)\big(k_y+Q_y\big)}{2}+ik_x\big(k_y+Q_y\big)\right]. \tag{A.3}$$

Thus, we have

$$\varphi_0(x,y)\varphi_0^*\big(x-k_y,y+k_x\big)$$
$$= exp\{-ixk_x\}\sum_{Q_1\tilde{d}_1+Q_2\tilde{d}_2} exp\big[i(k_x+Q_x)x$$
$$+ i\big(k_y+Q_y\big)y\big]exp\left[\frac{\pi i}{2}(Q_1^2+Q_1)\right]exp\left[-\frac{(\boldsymbol{k}+\boldsymbol{Q})^2}{4}\right.$$
$$\left.-\frac{i(k_x+Q_x)\big(k_y+Q_y\big)}{2}+ik_x\big(k_y+Q_y\big)\right]. \tag{A.4}$$

We can rewrite Eq.(A.1) by using Eq.(A.2)

$$\rho(x,y) = \sum_{\boldsymbol{k},\boldsymbol{l}} C_{\boldsymbol{k}}^{*} C_{\boldsymbol{l}}\, \varphi_{\boldsymbol{k}}^{*} \varphi_{\boldsymbol{l}}$$

$$= \sum_{\boldsymbol{k},\boldsymbol{l}} C_{\boldsymbol{k}}^{*} C_{\boldsymbol{l}}\ exp\{ix(k_x - l_x)\}\varphi_0^{*}(x - k_y, y + k_x)\varphi_0(x - l_y, y + l_x).$$

(A.5)

The two function product is

$$\varphi_0(x - l_y, y + l_x)\varphi_0^{*}(x - k_y, y + k_x),$$

set $x' = x - l_y, y' = y + l_x$

and then

$$\varphi_0(x', y')\varphi_0^{*}\left(x' - (k_y - l_y), y' + (k_x - l_x)\right),$$

set $k_x{}' = k_x - l_x, k_y{}' = k_y - l_y$, we have

$$\varphi_0(x', y')\varphi_0^{*}(x' - k_y{}', y' + k_x{}')$$

$$= exp\{-ix'k_x{}'\} \sum_{\boldsymbol{Q}} exp\big[i(k_x{}' + Q_x)x'$$

$$+ i(k_y{}' + Q_y)y'\big] exp\left[\frac{\pi i}{2}(Q_1^2 + Q_1)\right] exp\left[-\frac{(\boldsymbol{k}' + \boldsymbol{Q})^2}{4}\right.$$

$$\left. - \frac{i(k_x{}' + Q_x)(k_y{}' + Q_y)}{2} + ik_x{}'(k_y{}' + Q_y)\right],$$

rewrite x', y' by x, y and $k_x{}', k_y{}'$ by k_x, k_y

$$\varphi_0(x-l_y, y+l_x)\varphi_0^*(x-k_y, y+k_x)$$

$$= exp\{-i(x-l_y)(k_x-l_x)\}\sum_{\boldsymbol{Q}} exp\big[i(k_x-l_x+Q_x)(x-l_y)$$

$$+ i(k_y-l_y+Q_y)(y+l_x)\big]exp\left[\frac{\pi i}{2}(Q_1^2+Q_1)\right]exp\left[-\frac{(\boldsymbol{k}-\boldsymbol{l}+\boldsymbol{Q})^2}{4}\right.$$

$$\left.-\frac{i(k_x-l_x+Q_x)(k_y-l_y+Q_y)}{2}+i(k_x-l_x)(k_y-l_y+Q_y)\right]$$

(A.6)

substituting Eq.(A.6) into Eq.(A.3)

$$\rho(x,y)=\sum_{\boldsymbol{k},\boldsymbol{l}} C_{\boldsymbol{k}}^* C_{\boldsymbol{l}}\ exp\{ix(k_x-l_x)\}\varphi_{\boldsymbol{0}}^*(x-k_y, y+k_x)\varphi_0(x-l_y, y+l_x)$$

$$=\sum_{\boldsymbol{k},\boldsymbol{l}}\sum_{\boldsymbol{Q}} exp\{ix(k_x-l_x)\}exp\{-i(x-l_y)(k_x-l_x)\}exp\big[i(k_x-l_x+Q_x)(x-l_y)$$

$$+ i(k_y-l_y+Q_y)(y+l_x)\big]exp\left[\frac{\pi i}{2}(Q_1^2+Q_1)\right]exp\left[-\frac{(\boldsymbol{k}-\boldsymbol{l}+\boldsymbol{Q})^2}{4}\right.$$

$$\left.-\frac{i(k_x-l_x+Q_x)(k_y-l_y+Q_y)}{2}+i(k_x-l_x)(k_y-l_y+Q_y)\right]C_{\boldsymbol{k}}^* C_{\boldsymbol{l}}$$

$$=\sum_{\boldsymbol{k},\boldsymbol{l}}\sum_{\boldsymbol{Q}} exp\{il_y(k_x-l_x)\}exp\big[i(k_x-l_x+Q_x)x-i(k_x-l_x+Q_x)l_y$$

$$+ i(k_y-l_y+Q_y)y$$

$$+ i(k_y-l_y+Q_y)l_x\big]exp\left[\frac{\pi i}{2}(Q_1^2+Q_1)\right]exp\left[-\frac{(\boldsymbol{k}-\boldsymbol{l}+\boldsymbol{Q})^2}{4}\right.$$

$$\left.-\frac{i(k_x-l_x+Q_x)(k_y-l_y+Q_y)}{2}+i(k_x-l_x)(k_y-l_y+Q_y)\right]C_{\boldsymbol{k}}^* C_{\boldsymbol{l}}$$

$$= \sum_{\boldsymbol{k},\boldsymbol{l}} \sum_{\boldsymbol{Q}} exp\{il_y(k_x - l_x)\} exp\big[i(k_x - l_x + Q_x)x - i(k_x - l_x + Q_x)l_y$$

$$+ i\big(k_y - l_y + Q_y\big)y\big] exp\left[\frac{\pi i}{2}(Q_1^2 + Q_1)\right] exp\left[-\frac{(\boldsymbol{k} - \boldsymbol{l} + \boldsymbol{Q})^2}{4}\right.$$

$$\left. - \frac{i(k_x - l_x + Q_x)\big(k_y - l_y + Q_y\big)}{2} + ik_x\big(k_y - l_y + Q_y\big)\right] C_{\boldsymbol{k}}^* C_{\boldsymbol{l}}\,. \tag{A.7}$$

And then calulated $\tilde{\rho}(x, y)$ as the fourier transform of $\rho(x, y)$

We start from the equation of $|\psi(x, y)|^2$

$$\rho(x, y) = \sum_{\boldsymbol{k},\boldsymbol{l}} \sum_{\boldsymbol{Q}} exp\{il_y(k_x - l_x)\} exp\big[i(k_x - l_x + Q_x)x + i\big(k_y - l_y + Q_y\big)y$$

$$- i(k_x - l_x + Q_x)l_y\big] exp\left[\frac{i\pi}{2}(Q_1^2 - Q_1)\right] exp\left[-\frac{(\boldsymbol{k} - \boldsymbol{l} + \boldsymbol{Q})^2}{4}\right.$$

$$\left. - \frac{i(k_x - l_x + Q_x)\big(k_y - l_y + Q_y\big)}{2} + ik_x\big(k_y - l_y + Q_y\big)\right] C_{\boldsymbol{k}}^* C_{\boldsymbol{l}}, \tag{A.8}$$

and the Fourier transform of $\rho(x, y)$ is

$$\tilde{\rho}(x, y) = \frac{1}{2\pi L^2} \int dxdy exp[-i(\mathbf{p} + \mathbf{P})$$

$$\cdot \mathbf{r}] \sum_{\boldsymbol{k},\boldsymbol{l}} \sum_{\boldsymbol{Q}} exp\{il_y(k_x - l_x)\} exp\big[i(k_x - l_x + Q_x)x + i\big(k_y - l_y + Q_y\big)y$$

$$- i(k_x - l_x + Q_x)l_y\big] exp\left[\frac{i\pi}{2}(Q_1^2 - Q_1)\right] exp\left[-\frac{(\boldsymbol{k} - \boldsymbol{l} + \boldsymbol{Q})^2}{4}\right.$$

$$\left. - \frac{i(k_x - l_x + Q_x)\big(k_y - l_y + Q_y\big)}{2} + ik_x\big(k_y - l_y + Q_y\big)\right] C_{\boldsymbol{k}}^* C_{\boldsymbol{l}}\,. \tag{A.9}$$

Integration over x and y

$$\tilde{\rho}(\boldsymbol{p}+\boldsymbol{P}) = \sum_{\boldsymbol{k},\boldsymbol{l}} \sum_{\boldsymbol{Q}} \delta[\boldsymbol{p}+\boldsymbol{P}-(\boldsymbol{k}-\boldsymbol{l}+\boldsymbol{Q})] exp\{il_y(k_x-l_x)\} exp\big[i(k_x-l_x+Q_x)x + i\big(k_y-l_y+Q_y\big)y - i(k_x-l_x+Q_x)l_y\big] exp\left[\frac{i\pi}{2}(Q_1^2 - Q_1)\right] exp\left[-\frac{(\boldsymbol{k}-\boldsymbol{l}+\boldsymbol{Q})^2}{4} - \frac{i(k_x-l_x+Q_x)\big(k_y-l_y+Q_y\big)}{2} + ik_x\big(k_y-l_y+Q_y\big)\right] C_{\boldsymbol{k}}^* C_{\boldsymbol{l}}\,. \tag{A.10}$$

The Kronecker delta has four solutions :

$$\tilde{\rho} = \tilde{\rho}^{00} + \tilde{\rho}^{01} + \tilde{\rho}^{10} + \tilde{\rho}^{11}. \tag{A.11}$$

1. Major contribution $\tilde{\rho}^{00}$:

$$[p_1 + l_1 < 1 \ and \ p_2 + l_2 < 1]$$

$$Q_1 = P_1;\ k_1 = p_1 + l_1; Q_2 = P_2;\ k_2 = p_2 + l_2 \tag{A.12}$$

Substitute (B.5) into (B.3)

$$\tilde{\rho}^{00}(\boldsymbol{p}+\boldsymbol{P}) = \sum_{\boldsymbol{l}} exp\left\{i\pi\left[-P_1(2l_2-l_1) + \frac{1}{2}(p_1+2l_1-P_1)[2(p_2+P_2)-(p_1+P_1)]\right]\right\} exp\left[\frac{i\pi}{2}\left(P_1{}^2 - P_1\right)\right] exp\left[-\frac{(\boldsymbol{p}+\boldsymbol{P})^2}{4}\right] C^*_{p_1+l_1,p_2+l_2} C_{\boldsymbol{l}}\,. \tag{A.13}$$

2. One umklapp contribution $\tilde{\rho}^{01}$:

$$[p_1 + l_1 > 1 \ and \ p_2 + l_2 < 1]$$

$$Q_1 = P_1 + 1;\ k_1 = p_1 + l_1 - 1; Q_2 = P_2;\ k_2 = p_2 + l_2$$

(A.14)

Substitute (B.7) into (B.3)

$$\tilde{\rho}^{01}(\boldsymbol{p}+\boldsymbol{P}) = \sum_{\boldsymbol{l}} exp\left\{i\pi\left[-(P_1+1)(2l_2-l_1)\right.\right.$$

$$\left.\left.+\frac{1}{2}(p_1+2l_1-P_1-2)[2(p_2+P_2)-(p_1+P_1)]\right]\right\} exp\left\{\frac{i\pi}{2}[(P_1+1)^2\right.$$

$$\left.-(P_1+1)]\right\} exp\left[-\frac{(\boldsymbol{p}+\boldsymbol{P})^2}{4}\right] C^*_{p_1+l_1-1,p_2+l_2} C_{\boldsymbol{l}}\,.$$

(A.15)

3. One umklapp contribution $\tilde{\rho}^{10}$:

$$[p_1 + l_1 < 1 \ and \ p_2 + l_2 > 1]$$

$$Q_1 = P_1;\ k_1 = p_1 + l_1; Q_2 = P_2 + 1;\ k_2 = p_2 + l_2 - 1$$

(A.16)

Substitute (B.10) into (B.3)

$$\tilde{\rho}^{10}(\boldsymbol{p}+\boldsymbol{P}) = \sum_{\boldsymbol{l}} exp\left\{i\pi\left[-P_1(2l_2-l_1)\right.\right.$$

$$\left.\left.+\frac{1}{2}(p_1+2l_1-P_1)[2(p_2+P_2)-(p_1+P_1)]\right]\right\} exp\left[\frac{i\pi}{2}\left({P_1}^2\right.\right.$$

$$\left.\left.-P_1\right)\right] exp\left[-\frac{(\boldsymbol{p}+\boldsymbol{P})^2}{4}\right] C^*_{p_1+l_1,p_2+l_2-1} C_{\boldsymbol{l}}\,.$$

(A.17)

4. The two umklapp contribution $\tilde{\rho}^{11}$:

$$[p_1 + l_1 > 1 \ and \ p_2 + l_2 > 1]$$

$$Q_1 = P_1 + 1;\ k_1 = p_1 + l_1 - 1; Q_2 = P_2 + 1;\ k_2 = p_2 + l_2 - 1$$

(A.18)

Substitute (B.11) into (B.3)

$$\tilde{\rho}\ (\boldsymbol{p} + \boldsymbol{P}) = \sum_{\boldsymbol{l}} exp\left\{i\pi\left[-(P_1 + 1)(2l_2 - l_1)\right.\right.$$

$$\left.\left. + \frac{1}{2}(p_1 + 2l_1 - P_1 - 2)[2(p_2 + P_2) - (p_1 + P_1)]\right]\right\} exp\left\{\frac{i\pi}{2}[(P_1 + 1)^2\right.$$

$$\left. - (P_1 + 1)]\right\} exp\left[-\frac{(\boldsymbol{p} + \boldsymbol{P})^2}{4}\right] C^*_{p_1+l_1-1,p_2+l_2-1} C_{\boldsymbol{l}}\ .$$

(A.19)

Finally, we putted all contributions together with two conditions :

1. $if\ \ (p_1 + l_1) < 1 \rightarrow P' = P_1, P'' = P_1$

2. $if\ \ (p_1 + l_1) > 1 \rightarrow P' = P_1 + 1, P'' = P_1 + 2$

and we obtain

$$\tilde{\rho}(\boldsymbol{p} + \boldsymbol{P}) = \sum_{\boldsymbol{l}} exp\left\{i\pi\left[-P'(2l_2 - l_1)\right.\right.$$

$$\left.\left. + \frac{1}{2}(p_1 + 2l_1 - P'')[2(p_2 + P_2) - (p_1 + P_1)]\right]\right\} exp\left[\frac{i\pi}{2}(P'^2\right.$$

$$\left. - P')\right] exp\left[-\frac{(\boldsymbol{p} + \boldsymbol{P})^2}{4}\right] C^*_{[p_1+l_1],[p_2+l_2]} C_{\boldsymbol{l}}\ .$$

(A.20)

here $C_{[p_1+l_1]}$ indicates $C_{(p_1+l_1\ mod\ L)}$.

with two conditions :

1. $if\ \ (p_1 + l_1) < 1 \rightarrow P' = P_1, P'' = P_1$,

2. $if\ \ (p_1 + l_1) > 1 \rightarrow P' = P_1 + 1, P'' = P_1 + 2$.

Thus, the inverse Fourier transform of $\tilde{\rho}(x, y)$ is

$$\rho(x, y) = \sum_{\boldsymbol{p}+\boldsymbol{P}} \tilde{\rho}(\boldsymbol{p} + \boldsymbol{P}) exp[i(\boldsymbol{p} + \boldsymbol{P}) \cdot \boldsymbol{r}] . \qquad \text{(A.21)}$$

We turn back to calculate the terms of GL free energy.

Quadratic term

$$\frac{1}{4\pi}\int_{x,y} a_T|\Psi(x,y)|^2 = \frac{a_T}{4\pi}\int_{x,y}\sum_{\boldsymbol{p}+\boldsymbol{P}} \tilde{\rho}(\boldsymbol{p}+\boldsymbol{P}) exp[i(\boldsymbol{p}+\boldsymbol{P})\cdot\boldsymbol{r}] = \frac{a_T}{4\pi}[2\pi L^2\tilde{\rho}(\boldsymbol{0})]$$

$$= \frac{a_T}{2} L^2 \sum_{l} C_l^* C_l .$$

(A.22)

Quartic term

$$\frac{1}{8\pi}\int_{x,y} |\Psi(x,y)|^4$$

$$= \frac{1}{8\pi}\int_{x,y}\sum_{\boldsymbol{p}+\boldsymbol{P}} \tilde{\rho}(\boldsymbol{p}+\boldsymbol{P}) exp[i(\boldsymbol{p}+\boldsymbol{P})$$

$$\cdot \boldsymbol{r}] \sum_{\boldsymbol{p}'+\boldsymbol{P}'} \tilde{\rho}(\boldsymbol{p}'+\boldsymbol{P}') exp[i(\boldsymbol{p}'+\boldsymbol{P}')\cdot\boldsymbol{r}] = \frac{1}{4} L^2 \sum_{\boldsymbol{p}+\boldsymbol{P}} \tilde{\rho}(\boldsymbol{p}+\boldsymbol{P})\tilde{\rho}^*(\boldsymbol{p}+\boldsymbol{P})$$

$$= \frac{1}{4} L^2 \sum_{\boldsymbol{p}+\boldsymbol{P}} |\tilde{\rho}(\boldsymbol{p}+\boldsymbol{P})|^2 .$$

(A.23)

Substitute (A.19) into (A.23), we have

$$\frac{1}{8\pi}\int_{x,y}|\Psi(x,y)|^4$$

$$= \frac{1}{4}L^2\sum_{\boldsymbol{p},\boldsymbol{P}}\left|\sum_{\boldsymbol{l}} exp\left\{i\pi\left[-P'(2l_2-l_1)\right.\right.\right.$$

$$\left.\left.\left.+\frac{1}{2}(p_1+2l_1-P'')[2(p_2+P_2)-(p_1+P_1)]\right]\right\} exp\left[\frac{i\pi}{2}(\ ''^2\right.$$

$$\left.-P')\right] exp\left[-\frac{(\boldsymbol{p}+\boldsymbol{P})^2}{4}\right] C^*_{[p_1+l_1],[p_2+l_2]}C_{\boldsymbol{l}}\Bigg|^2 .$$

(A.24)

Appendix B

I used the random potential in the disorder term of GL equation as

$$U(x,y) = a_{0,0,0,0}$$

$$+ \sum_{p_1>0,P_1\geq 0,p_2=0,P_2=0}\{a_{p_1,0,P_1,0}exp[i(\boldsymbol{p}+\boldsymbol{P})\cdot\boldsymbol{r}]$$

$$+ a^*_{p_1,0,P_1,0}exp[-i(\boldsymbol{p}+\boldsymbol{P})\cdot\boldsymbol{r}]\}$$

$$+ \sum_{p_2+P_2>0}\{a_{\boldsymbol{p},\boldsymbol{P}}exp[i(\boldsymbol{p}+\boldsymbol{P})\cdot\boldsymbol{r}] + a^*_{\boldsymbol{p},\boldsymbol{P}}exp[-i(\boldsymbol{p}+\boldsymbol{P})\cdot\boldsymbol{r}]\}.$$

(B.1)

here a is the complex random numbers, $a_{\boldsymbol{p}+\boldsymbol{P}} = a_{-(\boldsymbol{p}+\boldsymbol{P})}$

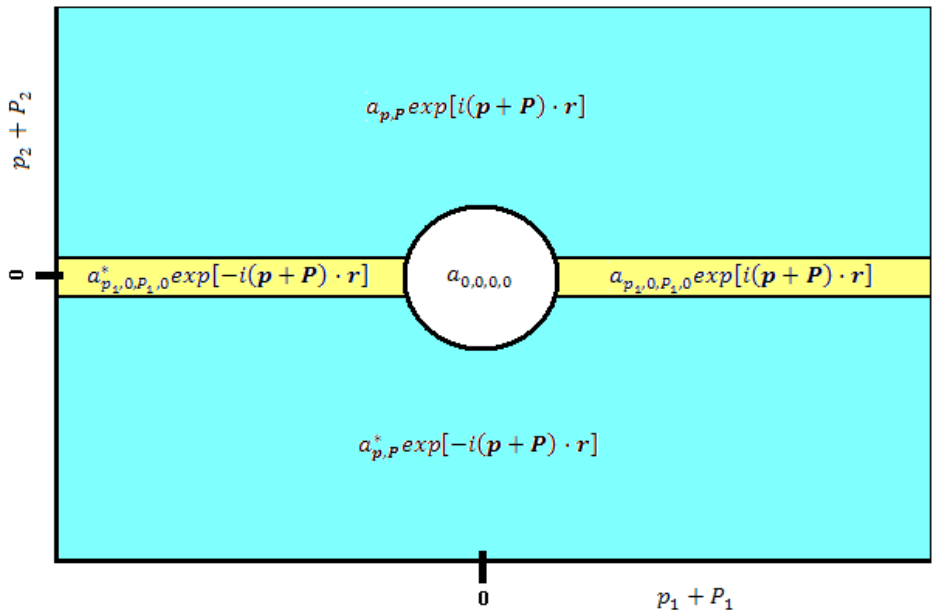

The distribution of the random potential in momentum space

and its distribution is divided into five parts. The white noise correlator is

$$\overline{U(x,y)U(0,0)} = \overline{a^2_{0,0,0,0}} + \sum_{p_1>0,P_1\geq 0,p_2=0,P_2=0} \{a^*_{p_1,0,P_1,0}a_{p_1,0,P_1,0}exp[i(\boldsymbol{p}+\boldsymbol{P})\cdot\boldsymbol{r}] + a^*_{p_1,0,P_1,0}a_{p_1,0,P_1,0}exp[-i(\boldsymbol{p}+\boldsymbol{P})\cdot\boldsymbol{r}]\} + \sum_{p_2+P_2>0} \{a^*_{\boldsymbol{p},\boldsymbol{P}}a_{\boldsymbol{p},\boldsymbol{P}}exp[i(\boldsymbol{p}+\boldsymbol{P})\cdot\boldsymbol{r}] + a^*_{\boldsymbol{p},\boldsymbol{P}}a_{\boldsymbol{p},\boldsymbol{P}}exp[-i(\boldsymbol{p}+\boldsymbol{P})\cdot\boldsymbol{r}]\}. \quad \text{(B.2)}$$

with some basic relations as follows:

$$\overline{a^2_{0,0,0,0}} = \frac{R}{2\pi L^2},$$

$$\overline{Rea^2} = \overline{Ima^2} = \frac{1}{2}\frac{R}{2\pi L^2} = \sigma^2, \quad \text{(B.3)}$$

here σ^2 is the variance of the normal distribution.

The disorder term of dimensionless GL free energy equation is

$$\int_{x,y} W(x,y)|\Psi(x,y)|^2$$

$$= 2\pi L^2 \frac{l\alpha T_c(1-t)}{2(\pi b' T)^{1/2}} \left\{ \tilde{\rho}(0) a_{0,0,0,0} \right.$$

$$+ \sum_{p_1>0, P_1\geq 0, p_2=0, P_2=0} \{\tilde{\rho}(\boldsymbol{p}+\boldsymbol{P}) a^*_{p_1,0,P_1,0} + c.c.\}$$

$$\left. + \sum_{p_2+P_2>0} \{\tilde{\rho}(\boldsymbol{p}+\boldsymbol{P}) a^*_{\boldsymbol{p},\boldsymbol{P}} + c.c.\} \right\}. \quad \text{(B.4)}$$

Appendix C

The energy of new configuration can be calculated by using

$$C_{l_1,l_2}^{new} = C_{l_1,l_2}^{old} + \delta_{l_1-j_1}\delta_{l_2-j_2}\Delta \tag{C.1}$$

Hence, the new superfluid density term is

$$\begin{aligned}
&\int_{x,y}^{\text{new}} |\Psi(x,y)|^2 = 2\pi L^2 \sum_{l_1,l_2} C_{l_1,l_2}^{new*} C_{l_1,l_2}^{new} \\
&= 2\pi L^2 \sum_{l_1,l_2} \left(C_{l_1,l_2} C_{l_1,l_2}^{old} + \delta_{l_1-j_1}\delta_{l_2-j_2}\Delta\right)^* \left(C_{l_1,l_2}^{old} + \delta_{l_1-j_1}\delta_{l_2-j_2}\Delta\right) \\
&= 2\pi L^2 \sum_{l_1,l_2} \left(C_{l_1,l_2}^{old} C_{l_1,l_2}^{old*} + C_{j_1,j_2}^{old*}\Delta + C_{j_1,j_2}^{old}\Delta^* + \Delta\Delta^*\right) \\
&= \int_{x,y}^{\text{old}} |\Psi(x,y)|^2 + 2\pi L^2 \left(C_{j_1,j_2}^{old*}\Delta + C_{j_1,j_2}^{old}\Delta^* + \Delta\Delta^*\right).
\end{aligned} \tag{C.2}$$

According to Eq.(A.23) and Eq.(b.4), we can obtain the new interaction term and disorder term by calculating $\tilde{\rho}(\boldsymbol{p}+\boldsymbol{P})$, so that

$$\begin{aligned}
\tilde{\rho}(\boldsymbol{p}+\boldsymbol{P}) = \sum_{\boldsymbol{l}} exp\Bigg\{ i\pi \Bigg[&-P'(2l_2 - l_1) \\
&+ \frac{1}{2}(p_1 + 2l_1 - P'')[2(p_2+P_2) - (p_1+P_1)] \Bigg] \Bigg\} exp\left[\frac{i\pi}{2}(P'^2 \right. \\
&\left. - P')\right] exp\left[-\frac{(\boldsymbol{p}+\boldsymbol{P})^2}{4}\right] \left(C_{[p_1+l_1],[p_2+l_2]}^{old*} + \delta_{[p_1+l_1]-j_1}\delta_{[p_2+l_2]-j_2}\Delta^*\right)\left(C_{l_1,l_2}^{old} \right. \\
&\left. + \delta_{l_1-j_1}\delta_{l_2-j_2}\Delta\right).
\end{aligned} \tag{C.3}$$

This calculation result can be separated into four part for different delta function solutions

as follows

(a)

$$\sum_{\boldsymbol{l}} exp\left\{i\pi\left[-P'(2l_2-l_1)+\frac{1}{2}(p_1+2l_1-P'')[2(p_2+P_2)-(p_1+P_1)]\right]\right\} exp\left[\frac{i\pi}{2}(P'^2 - P')\right] exp\left[-\frac{(\boldsymbol{p}+\boldsymbol{P})^2}{4}\right]\left(C^{old*}_{[p_1+l_1],[p_2+l_2]}C^{old}_{l_1,l_2}\right). \tag{C.4}$$

(b)

$$\sum_{\boldsymbol{l}} exp\left\{i\pi\left[-P'(2l_2-l_1)+\frac{1}{2}(p_1+2l_1-P'')[2(p_2+P_2)-(p_1+P_1)]\right]\right\} exp\left[\frac{i\pi}{2}(P'^2 - P')\right] exp\left[-\frac{(\boldsymbol{p}+\boldsymbol{P})^2}{4}\right]\left(\delta_{[p_1+l_1]-j_1}\delta_{[p_2+l_2]-j_2}\Delta^* C^{old}_{l_1,l_2}\right)$$

$$= exp\left\{i\pi\left[-P'(2[j_2-p_2]-[j_1-p_1]) + \frac{1}{2}(p_1+2[j_1-p_1]-P'')[2(p_2+P_2)-(p_1+P_1)]\right]\right\} exp\left[\frac{i\pi}{2}(P'^2 - P')\right] exp\left[-\frac{(\boldsymbol{p}+\boldsymbol{P})^2}{4}\right]\left(C^{old}_{[j_1-p_1],[j_2-p_2]}\Delta^*\right). \tag{C.5}$$

(c)

$$\tilde{\rho}(\boldsymbol{p}+\boldsymbol{P}) = \sum_{\boldsymbol{l}} exp\left\{i\pi\left[-P'(2l_2-l_1) + \frac{1}{2}(p_1+2l_1-P'')[2(p_2+P_2)-(p_1+P_1)]\right]\right\} exp\left[\frac{i\pi}{2}(P'^2 - P')\right] exp\left[-\frac{(\boldsymbol{p}+\boldsymbol{P})^2}{4}\right]\left(C^{old*}_{[p_1+l_1],[p_2+l_2]}\delta_{l_1-j_1}\delta_{l_2-j_2}\Delta\right)$$

$$= exp\left\{i\pi\left[-P'(2j_2 - j_1) + \frac{1}{2}(p_1 + 2j_1 - P'')[2(p_2 + P_2) - (p_1 + P_1)]\right]\right\} exp\left[\frac{i\pi}{2}(P'^2 - P')\right] exp\left[-\frac{(\boldsymbol{p} + \boldsymbol{P})^2}{4}\right]\left(C^{old*}_{[p_1+j_1],[p_2+j_2]}\Delta\right).$$

(C.6)

(d)

$$\sum_{l} exp\left\{i\pi\left[-P'(2l_2 - l_1) + \frac{1}{2}(p_1 + 2l_1 - P'')[2(p_2 + P_2) - (p_1 + P_1)]\right]\right\} exp\left[\frac{i\pi}{2}(P'^2 - P')\right] exp\left[-\frac{(\boldsymbol{p} + \boldsymbol{P})^2}{4}\right]\left(\delta_{[p_1+l_1]-j_1}\delta_{[p_2+l_2]-j_2}\delta_{l_1-j_1}\delta_{l_2-j_2}\Delta\Delta^*\right)$$

$$= exp\left\{i\pi\left[-P'(2j_2 - j_1) + \frac{1}{2}(2j_1 - P'')[2(P_2) - (P_1)]\right]\right\} exp\left[\frac{i\pi}{2}(P'^2 - P')\right] exp\left[-\frac{(\boldsymbol{p} + \boldsymbol{P})^2}{4}\right](\Delta\Delta^*).$$

(C.7)

Finally, we substitute Eq.(C.4) ~ Eq.(C.7) into Eq.(C.3)

$$\tilde{\rho}(\boldsymbol{p} + \boldsymbol{P}) = \sum_{l} exp\left\{i\pi\left[-P'(2l_2 - l_1) + \frac{1}{2}(p_1 + 2l_1 - P'')[2(p_2 + P_2) - (p_1 + P_1)]\right]\right\} exp\left[\frac{i\pi}{2}(P'^2 - P')\right] exp\left[-\frac{(\boldsymbol{p} + \boldsymbol{P})^2}{4}\right]\left(C^{old*}_{[p_1+l_1],[p_2+l_2]}C^{old}_{l_1,l_2}\right)$$

$$+ exp\left\{i\pi\left[-P'(2[j_2 - p_2] - [j_1 - p_1])\right.\right.$$

$$\left.\left.+\frac{1}{2}(p_1 + 2[j_1 - p_1] - P'')[2(p_2 + P_2) - (p_1 + P_1)]\right]\right\} exp\left[\frac{i\pi}{2}(P'^2\right.$$

$$\left.- P')\right] exp\left[-\frac{(\boldsymbol{p} + \boldsymbol{P})^2}{4}\right]\left(C^{old}_{[j_1 - p_1],[j_2 - p_2]}\Delta^*\right)$$

$$+ exp\left\{i\pi\left[-P'(2j_2 - j_1) + \frac{1}{2}(p_1 + 2j_1 - P'')[2(p_2 + P_2) - (p_1 + P_1)]\right]\right\} exp\left[\frac{i\pi}{2}(P'^2\right.$$

$$\left.- P')\right] exp\left[-\frac{(\boldsymbol{p} + \boldsymbol{P})^2}{4}\right]\left(C^{old*}_{[p_1 + j_1],[p_2 + j_2]}\Delta\right)$$

$$+ exp\left\{i\pi\left[-P'(2j_2 - j_1) + \frac{1}{2}(2j_1 - P'')[2(P_2) - (P_1)]\right]\right\} exp\left[\frac{i\pi}{2}(P'^2\right.$$

$$\left.- P')\right] exp\left[-\frac{(\boldsymbol{p} + \boldsymbol{P})^2}{4}\right](\Delta\Delta^*). \qquad \text{(C.8)}$$

Reference

[1] A. A. Abrikosov, Zh. Eksp. Teor. Fiz. 32, 1442 Sov. Phys. JETP 5, 1174 (1957).

[2] B. Rosenstein, D. Li and Valery M. Vinokur, AIP Conf. Proc. **850**, 871 (2006).

[3] A. P Levanyuk, Zh. Eksp. Teor. Fiz. **36**, 810 (1959).

[4] V. L.Ginzburg, Fiz. Tverd. Tela _Leningrad_ **2**, 203 _Sov. Phys. Solid State **2**, 1824 (1960).

[5] Larkin, A., and A. Varlamov, "Theory of Fluctuations in Superconductors (Oxford University Press, New York)", (2005).

[6] D. Li and B. Rosenstein, Phys. Rev. B 65, 220504(R) (2002).

[7] D. Li and B. Rosenstein, Phys. Rev. Lett. 90, 167004 (2003).

[8] E. Zeldov, D. Majer, M. Konczykowski, V. B. Geshkenbein, V. M. Vinokur, and H. Shtrikman, Nature _London_ **375**, 373 (1995).

[9] M. Willemin, A. Schilling, H. Keller, C. Rossel, J. Hofer, U. Welp, W. K. Kwok, R. J. Olsson, and G. W. Crabtree, Phys. Rev. Lett. **81**, 4236 (1998).

[10] T. Nishizaki, K. Shibata, T. Sasaki, and N. Kobayashi, Physica C **341-348**, 957 (2000).

[11] H. Beidenkopf, N. Avraham, Y. Myasoedov, H. Shtrikman, E. Zeldov, B. Rosenstein, E. H. Brandt, and T. Tamegai, Phys. Rev. Lett. **95**, 257004 (2005).

[12] H. Beidenkopf, T. Verdene, Y. Myasoedov, H. Shtrikman, E. Zeldov, B. Rosenstein, D. Li, and T. Tamegai, Phys. Rev. Lett. **98**, 167004 (2007).

[13] A. Schilling, R. A. Fisher, N. E. Phillips, U. Welp, D. Dasgupta, W. K. Kwok, and G. W. Crabtree, Nature(London) **382**, 791 (1996).

[14] A. Schilling, R. A. Fisher, N. E. Phillips, U. Welp, W. K. Kwok, and G. W. Crabtree, Phys. Rev. Lett. **78**, 4833 (1997).

[15] F. Bouquet, C. Marcenat, E. Steep, R. Calemczuk, W. K. Kwok, U. Welp, G. W. Crabtree, R. A. Fisher, N. E. Phillips, and A. Schilling, Nature(London) **411**, 448 (2001).

[16] R. Lortz, F. Lin, N. Musolino, Y. Wang, A. Junod, B. Rosenstein, and N. Toyota, Phys. Rev. B **74**, 104502 (2006).

[17] R. Lortz, N. Musolino, Y. Wang, A. Junod, and N. Toyota, Phys. Rev. B **75**, 094503

(2007).

[18] A. I. Larkin, Zh. Eksp. Teor. Fiz. **58**, 1466 (1970).

[19] T. Giamarchi and P. Le Doussal, Phys. Rev. B 55, 6577 (1997).

[20] M. P. A. Fisher, Phys. Rev. Lett. 62, 1415 (1989).

[21] D. S. Fisher, M. P. A. Fisher, and D. A. Huse, Phys. Rev. B 43, 130 (1991).

[22] M. Feigelman, V. Geshkenbein, A. Larkin, and V. Vinokur, Phys. Rev. Lett. **63**, 2303 (1989).

[23] D. Li and B. Rosenstein, Phys. Rev. B. 60, 9704 (1999)

[24] B. Rosenstein and D. Li, Rev. Mod. Phys. 82, 109–168 (2010)

[25] H. Y. Lin, "Thermal fluctuations and disorder in 2D Ginzburg-Landau model", 國立交通大學, 碩士論文 (2007).

[26] T. Natterman and M. S. Li, Phys. Rev. Left. 71,432, (1993)

[27] Y. Kato and N. Nagaosa, Phys. Rev. B 48, 7383, (1993).

[28] D. P. Landau and K. Binder, “Monte Carlo simulation in Statistical Physics”, Cambridge, (2000)

[29] Y. Radzyner, A. Shaulov, Y. Yeshurun, I. Felner, K. Kishio, and J. Shimoyama, Phys. Rev. B 65, 214525 (2002)

[30] Y. Radzyner, A. Shaulov, and Y. Yeshurun , Phys. Rev. B 65, 100513 (2002)